Full title

Short-range interactions between fibrocytes and CD8$^+$ T cells in COPD bronchial inflammatory response

Short title

Interactions between fibrocytes and CD8$^+$ T cells in COPD lungs

Authors

Edmée Eyraud[1,2], Elise Maurat[1,2], Jean-Marc Sac-Epée[3], Pauline Henrot[1,2,4], Maeva Zysman[1,2,4], Pauline Esteves[1,2], Thomas Trian[1,2], Hugues Bégueret[1,2,4], Pierre-Oliver Girodet[1,2,4], Matthieu Thumerel[1,2,4], Romain Hustache-Castaing[1,2,4], Roger Marthan[1,2,4], Florian Levet[5,6], Pierre Vallois[3], Cécile Contin-Bordes[7,8], Patrick Berger[1,2,4], Isabelle Dupin[1,2,*]

Affiliations

[1]Univ-Bordeaux, Centre de Recherche Cardio-thoracique de Bordeaux, U1045, Département de Pharmacologie, CIC1401, Pessac, France. [2]INSERM, Centre de Recherche Cardio-thoracique de Bordeaux, U1045, CIC1401, Pessac, France. [3]Univ-Lorraine, Institut Elie Cartan de Lorraine, UMR7502, Vandoeuvre-lès-Nancy, France. [4]CHU de Bordeaux, Service d'exploration fonctionnelle respiratoire, CIC1401, Pessac, France. [5]Univ. Bordeaux, CNRS, Interdisciplinary Institute for Neuroscience, IINS, UMR 5297, Bordeaux, France. [6]Univ. Bordeaux, CNRS, INSERM, Bordeaux Imaging Center, BIC, UAR3420, US 4, Bordeaux, France. [7]CNRS, UMR5164 ImmunoConcEpT, Université de Bordeaux, Bordeaux, France. [8]CHU de Bordeaux, Laboratoire d'Immunologie et Immunogénétique, Bordeaux, France

*** Corresponding author:** Pr Isabelle DUPIN, PhD
Centre de recherche Cardio-thoracique de Bordeaux INSERM U1045
PTIB - Hôpital Xavier Arnozan, Avenue du Haut Lévêque, 33600 PESSAC
e-mail: isabelle.dupin@u-bordeaux.fr

Abstract

The peri-bronchial zone of chronic obstructive pulmonary disease (COPD) is the site of extensive infiltration of immune cell, allowing persistent contacts between resident cells and immune cells. Tissue fibrocytes interaction with $CD8^+$ T cells and its consequences were investigated. We show that interactions beween both cell types are more frequent in distal airways from COPD patients compared to those of control subjects. Tissular $CD8^+$ T cells from COPD patients promote fibrocyte chemotaxis via the CXCL8-CXCR1/2 axis. $CD8^+$ T cells establish short-term interactions with fibrocytes, that trigger $CD8^+$ T cell proliferation in a CD54- and CD86-dependent manner, as well as pro-inflammatory cytokines production. A computational model accurately predicts histological *ex vivo* characteristics and allows to monitors disease evolution. Overall, our study reveals that local interactions between fibrocytes and $CD8^+$ T cells may comromise the balance between protective immunity and chronic inflammation in bronchi of COPD patients.

Teaser

Fibrocytes/$CD8^+$ T cells interactions cause inflammation through a maintained pathophysiological loop in bronchi of COPD patients.

MAIN TEXT

Introduction

The prevalence of COPD, one of the most common chronic diseases worldwide, has been rising in recent decades (*1*); thus, prevention and treatment of COPD are important issues of global healthcare. COPD bronchi are an area of intense immunological activity and tissue remodeling, as evidenced by the extensive immune cell infiltration and changes in tissue structures such as peribronchial fibrosis. In particular, distal airways are hypothesized to constitute a "quiet zone", where exaggerated remodeling and inflammatory processes take place early in the history of the disease, without identifiable symptoms or lung function tests alteration (*2*, *3*). In these particular areas, persistent contacts occur between resident cells and stimulated immune cells migrating from the peripheral circulation to the distal airways. The relevance of direct contact between T cells and monocyte-macrophages to potentiate the inflammatory response has been demonstrated in many chronic inflammatory diseases affecting the central nervous system, osteoarticular structures and the lungs (*4*), but remains to be fully investigated in COPD.

Fibrocytes, fibroblast-like cells from the monocyte-macrophage lineage, produced by the bone marrow and released in the peripheral circulation, are recruited in the blood of COPD patients during an acute exacerbation (*5*). High circulating fibrocyte count during a COPD exacerbation is associated with an increased risk of death, suggesting that fibrocytes could be detrimental to the evolution of this disease (*5*). We have also demonstrated that tissue fibrocytes density increases in COPD bronchi, which was associated with a degraded lung function, increased wall thickness and air trapping (*6*). However, the function of these fibrocytes in COPD lungs is not yet fully understood. Besides their role in tissue scarring matrix production (*7*) and contraction (*8*), recruited fibrocytes may participate to lung inflammation in virtue of their immune properties. They can function as accessory cells in

the presentation of antigens to $CD4^+$ and $CD8^+$ T lymphocytes (*9*), and differentiated fibrocytes display a proteomic signature consistent with a strong engagement into immunomodulation (*10*). Cytotoxic $CD8^+$ T cells are predominant in the airways of COPD patients and their number inversely correlates with lung function (*11*). $CD8^+$ T cell-deficient mice are protected against lung inflammation and emphysema induced by cigarette smoke exposure (*12*) whereas the expression of molecules linked to tissue destruction, such as perforin, granzyme B and ADAM15, correlate with disease severity (*13*, *14*), suggesting $CD8^+$ T cells implication in lung inflammation and destruction in COPD. Activation of $CD8^+$ T cells is increased in COPD lung samples and has been shown to be smoking-independent (*15*, *16*). Other studies have shown that $CD8^+$ T cell activation could result from the exposure to self-antigens such as elastin fragments induced by cigarette smoke exposure (*17*), and could be partially T Cell Receptor (TCR)-independent (*13*). The absence of increased expression of cytotoxic enzyme in peripheral blood $CD8^+$ T cells from COPD patients argues in favor of a local activation within the lungs (*18*). $CD8^+$ T cells express an exhausted phenotype in the COPD lung, that may result from an over-activation thus participating to the defective response to infection in COPD (*19*, *20*). However, $CD8^+$ T cells activation's mechanism as well as their precise contribution to COPD pathogenesis remain largely unknown.

A recent study showed that fibrocytes, derived from the blood of lung adenocarcinoma patients, could strongly enhance the proliferation of $CD8^+$ T cells (*21*). We thus hypothesized that $CD8^+$ T cells and fibrocytes interact into the lungs, and that this interaction is critical in COPD pathology. Multiple immunostainings in combination with specific image analysis methods allow to determine the spatial distribution of individual $CD8^+$ T cells and fibrocytes within bronchial tissues of both control subjects and COPD patients. Using *in vitro* fibrocyte and CD8+ T cell–based experiments, we studied cell

interplay in terms of relative chemotaxis, dynamics, proliferation and cytokine secretion profile. We then integrated these findings into an agent-based computational model representing airways from either healthy or COPD patients enabling to test how local interactions shape spatial distributions of cell in both conditions. We propose that slight dysregulations of intercellular interactions induce abnormal cell organization around bronchi, ultimately causing a breakdown of tissue homeostasis, leading to chronic inflammation and tissue remodeling.

Results

Direct contacts between fibrocytes and CD8$^+$ T cells are more frequent in distal bronchial tissue from COPD patients than in that of controls

We used immunohistochemistry (IHC) to assess whether fibrocytes and CD8$^+$ T cells were in close vicinity in human tissue. Sections of distal lung tissues from 17 COPD and 25 control patients were obtained, from a previously described cohort (*6*), and labeled to detect CD8$^+$ T cells, identified as cells positive for CD8 staining and fibrocytes, identified as cells dual positive for FSP1 and CD45 double staining (fig. S1A-D). In agreement with previous studies (*6*, *11*, *22*), the density of both CD8$^+$ T cells and fibrocytes was increased within the subepithelial area of distal bronchi from COPD patients compared with that of control subjects (Fig. 1A-C). Moreover, fibrocytes and CD8$^+$ T cells were frequently in close proximity (Fig. 1D). To quantify the potential for cell–cell contacts, we determined the density of CD8$^+$ T cells in interaction with CD45$^+$ FSP1$^+$ cells (fig. S1A-D). Whatever the magnification used to automatically count interacting cells, the density of CD8$^+$ T cells in interaction with fibrocytes was higher in the sub-epithelial region of distal bronchi of COPD patients than in that of control subjects (Fig. 1D-F). For subsequent analyses, we chose the dilatation size "D8" (3.6 μm, which represents the radius of a mean ideal round cell in our analysis) to reflect the density of interacting cells. To evaluate the minimal distance between CD45$^+$ FSP1$^+$ cells and neighboring CD8$^+$ T cells, we used a CD8 distance map generated from the CD8 staining image, with the brightness of each pixel reflecting the distance from a CD8$^+$ T cell (fig. S1E-F). The mean minimal distance between fibrocytes and CD8$^+$ cells was significantly smaller in the sub-epithelial region of distal bronchi of COPD patients than in that of control subjects (Fig. 1G-H). In contrast, the mean minimal distances between CD8$^+$ T cells themselves or between fibrocytes themselves were unchanged (fig. S2A-B). The majority of both CD8$^+$ T cells and fibrocytes was located beneath the epithelium, with

their minimal distance and distribution relatively to the basal membrane being similar in control and COPD patients (fig. S2C-F). Altogether, no difference of spatial repartition was observed within each cell population between control and COPD patients, but the relative distribution of fibrocytes and $CD8^+$ cells was affected in tissues from patients with COPD.

To further describe the relative spatial organization of both cell types, we used a method based on Delaunay triangulation computed on previously segmented cell barycenters. It is based on a custom developed plugin to determine congregations of small groups of cells, called "clusters" (fig. S3). As expected from our minimal distance analysis, we found difference neither in the density of single cell-type clusters nor in their size, measured by the mean number of cells by cluster, between control subjects and patients with COPD (fig. 1I-J, left and middle panels). However, the density of clusters containing both cell types ("mixed cell clusters") was higher in distal bronchi of COPD patients than in those of control subjects, with a median number of 5 and 6 cells in these clusters in control and COPD tissues, respectively (Fig. 1I-J, right panels). This result indicates that fibrocytes and $CD8^+$ T cells are found within close proximity in the peribronchial area of COPD patients, with possible co-organization of $CD8^+$ T cells and fibrocytes in mixed cell clusters, indicating that direct and/or indirect fibrocyte-$CD8^+$ T cell interactions might occur *in vivo*.

Relationships between the density of $CD8^+$ T cells interacting with fibrocytes and functional parameters

We determined the univariate correlation coefficients between fibrocyte density, $CD8^+$ T cell density, the 3 variables quantifying the interaction of $CD8^+$ T cells with fibrocytes (the interacting cell density, the mean minimal distance between fibrocytes and $CD8^+$ T cells and the density of mixed cell clusters), and various functional and CT parameters (Tables S1 to S5). In particular, moderate but significant univariate correlations were found between

the Forced Expiratory Volume in 1 second / Forced Vital Capacity (FEV_1/FVC) ratio (used to diagnose COPD if below 0.7) and the density of fibrocytes, the density of interacting cells, the mean minimal distance between fibrocytes and $CD8^+$ T cells and the density of fibrocytes-$CD8^+$ T cells clusters (fig. S4A-D). Variables significantly correlated with FEV_1/FVC were entered into stepwise regression analyses in order to find the best model fitting FEV_1/FVC. The best model associated the density of interacting cells and the density of mixed cell clusters. It explained 35% of the FEV_1/FVC variability (Table S6). The relationships between the FEV_1/FVC ratio, the density of interacting cells and the density of mixed cell clusters were all statistically significant.

Chemo-attraction of $CD8^+$ T cells for fibrocytes is increased in COPD tissue

To decipher the molecular mechanisms underpinning the increased cell-cell interaction in COPD bronchi, we investigated cell adhesion and chemotaxis processes in $CD8^+$ T cells of patients with COPD compared with those of controls. Using the transcriptomic profile of tissular resident memory and effector memory $CD8^+$ T cells of COPD patients compared with that of control subjects in the GSE61397 microarray dataset (http://www.ncbi.nlm.nih.gov/geo/) published elsewhere (*23*), we noted significative changes in the abundance of transcripts of genes related to cell adhesion. However, the changes were not consistent with clear increased or decreased adhesive properties in both tissue resident memory $CD8^+$ $CD103^+$ T-cells (T_{RM}) and effector memory $CD8^+$ $CD103^-$ T-cells (T_{EM}) (fig. S5). In contrast, transcriptomic data reveal consistent changes in COPD cells *versus* controls, mostly increases, in chemokines and chemokine receptors (Fig. 2A). Most changes in transcripts were compatible with a pro-attractive and a pro-migratory response. In particular, there were increases of CCL2, CCL26, CXCL2 and CXCL8

187 expression in T_{RM} from patients with COPD, and CCL3L1 expression in T_{EM} from patients
188 with COPD (Fig. 2A).
189 We then investigated whether tissular $CD8^+$ T cells secretion from control or COPD patients
190 could affect fibrocytes migration in an *in vitro* assay (Fig. 2B). $CD8^+$ T cells were purified
191 from lung resection material sampled either in control subjects or in COPD patients, whose
192 characteristics are reported (Table S7). Precursors of fibrocytes were purified from blood
193 samples of a separate cohort of COPD patients (*i.e.*, COBRA), whose characteristics are
194 also reported (Table S8). The migration of fibrocytes was significantly increased by
195 conditioned medium derived from tissular $CD8^+$ T cells of COPD patients compared with
196 those from control lungs (Fig. 2C).
197 The secretory profile of these tissular $CD8^+$ T cells 36h after culture conditions with soluble
198 anti-CD3 and anti-CD28 antibodies was determined. The concentration of CXCL8 was
199 increased in $CD8^+$ T cells from COPD patients compared to control cells (Fig. 2D) in good
200 agreement with the transcriptomic analysis. By contrast, the concentration of both CCL3
201 and CCL3L1 was undetectable (data not shown), whereas that of CCL2 and CXCL2
202 remained unchanged (Fig. 2D). Since CXCL8 is a ligand of the chemokine receptors
203 CXCR1 and/or CXCR2, we repeated the migration assay with the addition of the drug
204 reparixin, an antagonist of both CXCR1 and CXCR2 (*24*). Whereas fibrocyte treatment with
205 reparixin had no significant effect on the control $CD8^+$ T cells-mediated migration, it did
206 inhibit the increased migration induced by the secretions of $CD8^+$ T cells purified from
207 COPD tissues (Fig. 2E). Moreover, an anti-CXCL8 blocking antibody also inhibited the
208 increased migration induced by the secretions of $CD8^+$ T cells purified from COPD tissues
209 (Fig. 2F). These data indicate that tissular $CD8^+$ T cells from patients with COPD promote
210 fibrocyte chemotaxis via CXCL8-CXCR1/2 axis.
211

CD8$^+$ T cells repeatedly interact with fibrocytes

As fibrocytes and CD8$^+$ T cells reside in close proximity in the subepithelial area, especially that of tissues from COPD patients, we investigated their crosstalk capacity. We developed an autologous *in vitro* co-culture system allowing precise control over the cell types involved. Fibrocytes and CD8$^+$ T cells, both purified from blood of COPD patients were co-cultured 2 days before image acquisition for the following 12h. CD8$^+$ T cells were either nonactivated or activated with anti-CD3/CD28 antibodies coated microbeads. At the beginning of live imaging, nonactivated CD8$^+$ T cells were equally allocated in fibrocyte-covered zones (41 ± 8%) and in fibrocyte-free zones (59% ± 8%) (Fig. 3A-B). Twelve h later, most (77 ± 9%) of CD8$^+$ T cells were present in contact with fibrocytes (Fig. 3A-B). Activation of CD8$^+$ T cells resulted in similar distribution (Fig. 3A-B). These data suggest that both cell types are able to directly interact, and that these interactions progressively increase during co-culture. We tracked individual CD8$^+$ T cells during 12h time lapse to capture their spatiotemporal dynamics using multiple variables quantification (Fig. 3C and Movie S1). For both nonactivated and activated lymphocytes, the mean speed of CD8$^+$ T cells decreased upon contact with fibrocytes (Fig. 3D). Irrespective of the activation state of CD8$^+$ T cells, a majority of intercellular contacts (49 ± 6% and 49 ± 8% for nonactivated and activated CD8$^+$ T cells, respectively) were short-lived (<12 min) and dynamic, although some longer interactions (>32 min) could also be detected (30 ± 4% and 27 ± 7% for nonactivated and activated CD8$^+$ T cells, respectively) (Fig. 3E). The contact coefficient and the mean velocity of CD8$^+$ T cells measured in the absence of contact with fibrocytes ("Mean free speed") were similar in both conditions of activation (Fig. 3F-G). However, we observed a significant decrease in the mean speed for activated CD8$^+$ T cells when they were in contact with fibrocytes ("Mean contact speed") compared to nonactivated CD8$^+$ T cells (Fig. 3H), reflecting subtle behavior changes in this condition of activation.

Fibrocytes favor CD8$^+$ T cell proliferation in a cell-cell contact-dependent manner

Since multiple transient contacts have been shown to be an early trigger of events leading to clonal expansion (*25*), we wondered whether fibrocytes could promote CD8$^+$ T cells proliferation using total cell count and a CellTrace-based co-culture proliferation assay. We designed two different co-culture assays modeling either a direct contact between the two cell types or an indirect contact (transwell assay). The activation of CD8$^+$ T cells by anti-CD3/CD28 antibody coated microbeads slightly increased the basal level of dividing CD8$^+$ T cells (comparison of the conditions "$CD8_{NA}$" and "$CD8_A$" without fibrocytes in Fig. 3I-P). The presence of fibrocytes in the indirect co-culture assay did not affect proliferation capacity of non-activated CD8$^+$ T cells and only moderately increased the number of dividing activated CD8$^+$ T cells (Fig. 3 I-L). The distinction between naïve (CD45RA$^+$) and memory (CD45RA$^-$) CD8$^+$ T cells did not reveal any selective effect of fibrocytes on these two CD8$^+$ subpopulations (fig. S6A, C and S6E-H). In the direct co-culture model, the total number of CD8$^+$ T cells and the percentage of dividing CD8$^+$ T cells were far higher in the presence of fibrocytes irrespective of the activation state of CD8$^+$ T cells (Fig. 3M-P). This effect seemed to be particularly impressive for naïve CD8$^+$ T cells as they demonstrated an average differential of 80 ± 14% and 70 ± 20% of dividing cells between the conditions with and without fibrocytes, respectively for nonactivated (fig. S6I-J, top panels) and activated CD8$^+$ T cells (fig. S6I-J, bottom panels), *vs* 67 ± 18% and 52 ± 20% for memory CD8$^+$ T cells (fig. S6K-L). Altogether, this implies that a direct rather than indirect interactions between CD8$^+$ T cells and fibrocytes increased CD8$^+$ T cell proliferation.

After 6 days of co-culture, a cell population with a low level of CD8 expression (CD8^{low}) appeared, that was inversely proportional to the level of CD8$^+$ T cells strongly expressing a high level of CD8 (CD8^{high}, fig. S7). The CellTrace-based assay showed that those cells

highly proliferated during co-culture, especially in the direct co-culture (fig. S7E), suggesting that $CD8^{high}$ cells disappeared in favor of $CD8^{low}$ cells. As fibrocytes could have contaminated the cell suspension harvested from the direct co-culture, we did check that those $CD8^{low}$ cells were not $CD45^+$ Collagen I^+ (fig. S8). Phenotypic analysis of this $CD8^{low}$ population indicated that cells were mostly $CD45RA^-$ cells (fig. S7A-B, S7D-E), with a low level of cytokine expression (fig. S7C, F). Since $CD8^{low}$ cells may thus represent a population of exhausted T cells, we focused on $CD8^{high}$ cells in the following, especially regarding the secretion profile characterization. As CD86 and CD54 co-stimulatory molecule and adhesion molecule, respectively, pivotal in immunological synapse formation, are both expressed by fibrocytes (*21*, *26*), we tested the effects of anti-CD54 and anti-CD86 blocking antibodies on fibrocyte-induced proliferation of $CD8^+$ T cells. The inhibition of CD86 and CD54 significantly reduced proliferation of nonactivated $CD8^+$ T cells in the direct co-culture with fibrocytes (Fig. 4). However, these antibodies failed to alter the stimulatory activity of lymphocyte division by fibrocytes, when $CD8^+$ T cells were previously activated (Fig. 4). Blocking LFA-1 did not affect the fibrocyte-mediated $CD8^+$ T cell division (fig. S9A-D), suggesting the existence of compensatory integrins at the surface of the lymphocyte, such as CD11b/CD18, to mediate the interaction with CD54. The inhibition of CD44, a receptor for hyaluronan which has been shown to be produced by fibrocytes (*27*), did not impair the proliferation of $CD8^+$ T cells irrespective of their activation state (fig. S9E-H).

In total, these results indicate that direct contacts between fibrocytes and $CD8^+$ T cells, such as those mediated by CD54 and CD86, were strong positive signals to trigger $CD8^+$ T cell proliferation with the induction of $CD8^{high}$ and $CD8^{low}$ phenotypes.

Fibrocyte-$CD8^+$ T cell interactions alter cytokine production

Multiparametric flow cytometry was used to characterize the cytokine expression profile of $CD8^+$ T cells in the indirect and direct co-culture with fibrocytes. When nonactivated $CD8^+$ T cells were indirect co-cultured with fibrocytes, the expression of TNF-α, IFN-γ by $CD8^+$ T cells was slightly increased (Fig. 5A-B). IL-10, IL-17 and Granzyme B were not detected (Fig. 5A-B). When $CD8^+$ T cells were activated with anti-CD3/CD28, the level of TNF-α and IFN-γ further increased, and the expression of granzyme B and IL-10 was slightly induced (Fig. 5A-B). Upon direct co-culture, we observed a massive induction of TNF-α, IFN-γ, granzyme B, IL-10 and IL-17, irrespective of the activation state of $CD8^+$ T cells (Fig. 5C-D). Altogether, these results show that soluble factors and direct contacts between fibrocytes and $CD8^+$ T cells might have an additive effect on $CD8^+$ T cell cytokine production. The concentration of TNF-α measured in culture supernatant increased significantly upon co-culture between fibrocytes and non-activated $CD8^+$ T cells at day 4, confirming that TNF-α was secreted in the medium upon direct interactions with fibrocytes (Fig. 5E). This shows that both soluble factors produced by fibrocytes and direct contacts influence $CD8^+$ T cell secretion profile.

We then wondered whether glucocorticoid drugs (*i.e.*, budesonide or fluticasone propionate) could reverse the fibrocyte-induced proliferation and differentiation of $CD8^+$ T cells. Treatment with glucocorticoid drugs significantly decreased fibrocyte-induced TNF-α secretion by non-activated $CD8^+$ T cells, without affecting the proliferation (fig. S10). Collectively, these results underline the importance of the interaction with fibrocytes for $CD8^+$ T cell activation, possibly by favoring cellular proliferation and local cytokine production.

Stochastic mathematical model taking into account intercellular interactions describes the evolution over time of cell populations in control and COPD bronchi

All the above mentioned results led us to hypothesize that fibrocyte infiltration into the lung, differential migration of fibrocytes towards $CD8^+$ T cells and subsequent $CD8^+$ T cell proliferation, could result in a distinct spatial cellular repartition observed in tissues obtained from patients with COPD, compared to control tissues. To investigate this hypothesis, which could not be experimentally tested, we developed an agent-based (cellular automata) model with local and random cellular interactions. We considered the lamina propria (*i.e.*, the peribronchial zone), located between the bronchial epithelium and the smooth muscle layer, which contains fibrocytes and $CD8^+$ T cells. In line with the present analysis, the computational domain (*i.e.*, the lamina propria), corresponds to a zone of 179 000 μm^2. Fibrocytes and $CD8^+$ T cell are considered as individual objects that can move, divide, die and infiltrate the lamina propria at the stable state and during exacerbation. Their individual behaviors and interactions are supposed to be stochastic and the value of the probabilities has been established from literature (*5*, *6*, *10*, *21*, *28–41*) and the present *in vitro* data, as summarized in the method section and in Tables S9 and S10, and exhaustively described in the supplementary text and (*42*). Initial cell densities were scaled with respect to reference values, corresponding to the mean densities measured in non-smoking subjects. Simulations started with these initial densities and ended 20 years later, to reflect the average time between the beginning of cigarette smoke exposure and COPD onset (*43*).

All the biological processes are governed by probabilities (Fig. 6A). $CD8^+$ T cells, but not fibrocytes, are able to proliferate, based on our own unpublished observations and other studies (*10*, *34*). The presence of fibrocytes in the local neighborhood of a $CD8^+$ T cell can trigger $CD8^+$ T cell division with increased probability, based on the present *in vitro* experiments showing that the contact between those two cell types greatly enhanced $CD8^+$

T cell proliferation. Fibrocytes and $CD8^+$ T cells movements depend on the local neighborhood of cells, reflecting their relative chemo-attractive properties. We then simulated the evolution over 20 years, with two sets of parameters, respectively for the control and COPD cases and the second for the COPD case (see supplementary text).

We first tested the results of simulations against our experimental data from patients' tissues. First, we compared cell densities, experimentally measured in tissue samples, with theoretical predictions at the final state. Snapshots of the peribronchial area at the end of the simulations show that the densities of cells as well as their relative distribution were different between healthy and COPD situations (Fig. 6B). From the simulations (n=160 in each condition), we found a median of 754 $CD8^+$ T cells/mm^2 (95% CI, 748 to 763) and 106 fibrocytes/mm^2 (95% CI, 101 to 108) in the control situation, and 1187 $CD8^+$ T cells/mm^2 (95% CI, 1169 to 1195) and 212 fibrocytes/mm^2 (95% CI, 206 to 216) in the COPD situation. These values are in very good agreement with our experimental findings, and the simulations were also able to reproduce the statistical increase of cell densities in COPD situation compared to that of controls (Fig. 6C). Next, we tested if our theory accounted for the experimental relative distribution of $CD8^+$ T cells and fibrocytes. The densities of $CD8^+$ T cells in interaction with fibrocytes (Fig. 6D), the mean minimal distances between fibrocytes and $CD8^+$ cells (Fig. 6E), the distribution of mean minimal distances (fig. S11) and the mean number of mixed cell clusters (Fig. 6F) were in good agreement with tissular analyses and mimicked the variations observed between control subjects and patients with COPD. The densities of mixed cell clusters predicted by simulations (control simulations: median = 17 clusters/mm^2 (95% CI, 18 to 21), COPD simulations: median = 45 clusters/mm^2 (95% CI, 46 to 51), $P<0.001$) agreed perfectly with experimental measurements (Fig. 6G) and were therefore chosen as a readout of intercellular interactions in the following analyses. If purely random, the density of mixed clusters was

expected to be 28 clusters/µm^2 (95% CI, 25 to 29) and 73 clusters/µm^2 (95% CI, 70 to 74) in control and COPD situations, respectively (fig. S12). These random densities as well as the others parameters quantifying the relative distribution of cells were statistically different from the distributions obtained in both simulations and *in situ* analyses (fig. S12). We conclude that the relative organization of CD8$^+$ T cells and fibrocytes in control and COPD bronchi did not result from a pure stochastic mechanism but implicates chemotaxis processes.

One of the strengths of the model is to allow the monitoring of the temporal evolution of the different cellular processes and the numerical detection of a change of regime (Fig. 6H-I). CD8$^+$ T cells infiltration remained identical in control and COPD situation. Fibrocyte-induced T cell proliferation, that represents the minor part of the total proliferation in control situation, quickly increased in COPD situation over time to reach a plateau after approximately 4 years. As the basal proliferation of CD8$^+$ T cells remained similar in healthy and diseased situations, the resulting total proliferation in CD8$^+$ T cells over time was higher in the COPD situation compared to the control one. COPD dynamics also affected CD8$^+$ T cell death, with a concomitant increase of T cell-induced death. In total, the net balance between gain and loss of CD8$^+$ T cells was around zero for control dynamics and strictly positive for COPD dynamics, explaining the increased CD8$^+$ T cell density in COPD simulations. Fibrocytes infiltration remained very similar in control and COPD dynamics (Fig. 6I). Fibrocytes death was initially lower in COPD simulations before increasing and reaching a stationary state after approximately 7 years, resulting in a net expansion of fibrocytes population in COPD bronchi after 20 years. Moreover, the simulations allowed us to monitor the interactions between fibrocytes and CD8$^+$ T cells. The density of mixed cell clusters gradually increased in the first years of the COPD simulation before reaching a stationary state after approximately 6 years (Fig. 6J, Movies

S2 to S5). Altogether, the theory of the influence of local interactions tested by our agent-based (cellular automata) model correctly accounts for the shift of absolute and relative distribution of $CD8^+$ T cells and fibrocytes in peribronchial areas from control subjects to patients with COPD.

The above results constitute a validation of our model since for the different parameters considered, there is agreement between the simulations and the in vitro observations

Discussion

The present study aimed at identifying the role and mechanism of fibrocyte-$CD8^+$ T cells cross-talk in COPD. A previous study had pointed out a pivotal role for fibrocyte to activate $CD8^+$ T cells proliferation (*21*). However, whether and how both cell types could interact in bronchi, as well as their implication in COPD was completely unknown. Quantitative image analysis provided crucial insight into the relative distribution of fibrocytes and $CD8^+$ T cells in distal bronchial specimens from control subjects and COPD patients. In addition to data from previous studies demonstrating that the densities of both fibrocytes (*6*) and $CD8^+$ T cells (*41*) are increased within the distal bronchi of COPD patients, we found that fibrocyte and $CD8^+$ T cells are localized in close proximity in peribronchial areas, especially in tissues from patients with COPD. We deciphered the spatiotemporal characteristics of these cell–cell contacts by live imaging in an *in vitro* autologous co-culture assay, and showed that the duration of the contacts was compatible with activation through the establishment of dynamic synapses. On the one hand, $CD8^+$ T cells induced fibrocyte chemotaxis, and, on the other hand, fibrocytes directly induced $CD8^+$ T cell proliferation and cytokine production. The strength of our work relies on the integration of findings from

411 the present *in vitro* experiments and other studies into a comprehensive computational
412 model that provides an accurate prediction of histological *ex vivo* characteristics opening up
413 the possibility to figure out the *in vivo* effect of drugs in future studies. Altogether, our data
414 suggest a pivotal role for fibrocytes to activate $CD8^+$ T cell deleterious functions in the
415 context of COPD.
416
417 We analyzed the relationship between these histological parameters and clinical data and
418 found associations between fibrocyte presence, fibrocyte-$CD8^+$ T cell interaction and the
419 alteration of lung function. We have demonstrated using stepwise and multivariate
420 regressions that the density of interacting cells and the density of mixed cell cluster were
421 the two best correlated parameters with the FEV_1/FVC ratio, supporting a potential role for
422 the interplay between both cell types in COPD. Since regions of microscopic
423 emphysematous destruction of terminal bronchioles have been associated with increased
424 infiltration of $CD8^+$ T cells and immune response activation, such as the up-regulation of
425 IFN-γ signaling (*44*), it is tempting to speculate that fibrocyte-$CD8^+$ T cell interplay could
426 be implicated in early changes leading to tissue remodeling and chronic inflammation in
427 COPD. Of note, the gene signature obtained by tissue microarray associated with this site
428 also indicates the modification of two genes associated with the tissue repair process, FGF10
429 and TGFB2 (*44*). Considering the possible effect of $CD8^+$ T cells on fibrocyte
430 differentiation, it could be worthwhile to focus on these genes in further studies.
431
432 We also addressed the potential mechanisms explaining these increased interactions of
433 $CD8^+$ T cells and fibrocytes in tissues of COPD patients. Chemotaxis could guide $CD8^+$ T
434 cells towards fibrocytes and reciprocally, as it has been proposed for T cells towards
435 dendritic cells (*45–47*). Stronger or longer interactions could also explain the differential

spatial distribution between healthy and diseased tissues. On the other hand, the contact between both cell types could also occur through a stochastic mechanism, as shown for $CD4^+$ T cells and dendritic cells in lymph nodes, without any implication of chemotactic processes (*48*). Although we cannot totally rule out a role for fibrocyte-$CD8^+$ T cell adhesion to explain the increased interactions, our findings rather suggest a central role for the CXCL8-CXCR1/2 axis in promoting encounters between $CD8^+$ T cells and fibrocytes in COPD patients. Importantly, this is further supported by the results of computational modelization, which only integrates chemotaxis and not adhesion processes, revealing a final spatial repartition of cells in the COPD situation distinct from a random distribution. Altogether, our data suggest that the likelihood of interactions between fibrocytes and $CD8^+$ T cells could be increased in tissues from patients with COPD through the CXCL8-CXCR1/2 axis thus participating to cluster fibrocytes and $CD8^+$ T cells in diseased tissues. Importantly, dual blockers of CXCR1-CXCR2 have been suggested as therapeutic targets in COPD (*49*) and are efficient in our *in vitro* experiments to block the increased chemotaxis of fibrocytes towards secretion of $CD8^+$ T cells purified from COPD tissues. The outcome of such therapies could be predicted using the computational model described in this study.

We show that fibrocytes act as a major promoter on $CD8^+$ T cell proliferation, thus confirming, in an autologous co-culture system, what has been previously found in the context of cancer-related immunity (*21*). This is consistent with the present *in situ* analyses, showing the presence of clusters containing both cell types in peribronchial area, especially in the tissues from patients with COPD. The mean numbers of cells in those clusters remained relatively low, suggesting that these structures are distinct from inducible bronchus-associated lymphoid tissue (iBALT) (*50*). Although a previous report has demonstrated that fibrocytes, exposed to viral antigens, could induce proliferation of naïve

461 $CD8^+$ T cells (*26*), the pro-proliferative effect exerted by fibrocytes on $CD8^+$ T cells
462 occurred without antigen exposure in our *in vitro* study. This antigen-independent T cell
463 proliferation driven by fibrocytes was also found in the context of sepsis (*51*), suggesting
464 that fibrocytes generally impact T cells expansion with a mechanism independent of the
465 traditional antigen-driven clonal proliferation. This is also in agreement with our findings
466 showing that contacts between $CD8^+$ T cells and fibrocytes were relatively short and
467 dynamic, and that the dynamics of the interaction did not depend on the activation state of
468 $CD8^+$ T cells. The spatiotemporal behavior of $CD8^+$ T cells was consistent with the
469 establishment of dynamic synapse, also called "kinapse" (*52*), which are associated with the
470 induction of relatively weak TCR signals (*53*). We have evidenced the requirement for
471 cellular contacts, implicating the surface receptors CD86 and CD54. The lack of effect of
472 the anti-CD86 and CD54in pre-activated $CD8^+$ T cells might indicate potential changes of
473 expression of molecules belonging to the immunological synapse upon activation, that could
474 make the lymphocytes more responsive to others signals. The well-known inhaled
475 corticosteroids (*i.e.*, budesonide and fluticasone propionate) also failed to significantly
476 inhibit fibrocyte-induced $CD8^+$ T cell proliferation. This is consistent with their lack of
477 activity in lymphocytes obtained from patients with COPD (*54*). In contrast, we propose
478 that targeting the interaction between structural and immune cells and/or its consequences
479 should reveal robust candidates for future pharmacotherapeutic strategies to treat COPD. Of
480 note, the stimulatory activity of $CD8^+$ T cells by fibrocytes was also found to be enhanced
481 by the blockade of the PD-1/PD-L1 pathway in a previous study (*21*). As this latter property
482 of fibrocytes may be beneficial in tumor microenvironment (*55*), especially when cancer
483 patients were treated with anti–PD-1/PD-L1 antibody, it might be rather detrimental in
484 COPD patients, by promoting tissue damages and chronic immune inflammation.
485

Fibrocytes skewed $CD8^+$ T-cell populations towards both $CD8^{high}$ and $CD8^{low}$ phenotypes in a cell–cell contact independent manner. It has been described that, following contact between an antigen presenting cell and a lymphocyte, asymmetric division can occur generating a memory cell, weakly expressing CD8, and an effector cell strongly expressing CD8 (*56*, *57*). The asymmetry is reduced but still present even without specific recognition of foreign antigen by T cells (*57*). It is tempting to speculate that the induced proliferation we observed in our experiments generates, via asymmetric division, unequal CD8 inheritance in daughter cells. The low level of cytokine expression in $CD8^{low}$ cells is compatible with an exhausted phenotype, while $CD8^{high}$ cells express higher levels of cytokines, a profile consistent with an effector commitment. Although the presence of the $CD8^{high}$ and $CD8^{low}$ subsets remain to be evidenced in the tissues, we suspect that the relative expansion of the $CD8^{high}$ and $CD8^{low}$ subset triggered by fibrocytes could have functional implications. Reiterative rounds of $CD8^+$ T cells division induced by frequent interactions with fibrocytes might induce defective immune response by exhausted $CD8^{low}$ T cells (*19*, *20*), and tissue destruction by cytotoxic $CD8^{high}$ cells (*12*, *58*).

In COPD, outside of exacerbations, factors triggering pro-inflammatory cytokines production are still elusive. Here, we demonstrate that fibrocytes exert a strong effect through soluble factors and direct cellular contacts with $CD8^+$ T cells, inducing a massive upregulation of TNF-α, IFN-γ and granzyme B production, all implicated in COPD pathophysiology (*59*). Greater production of TNF-α, IFN-γ and granzyme B by $CD8^+$ T cells triggered by the interaction with fibrocytes is consistent with previous studies showing enhanced production of Tc1 cytokines and cytotoxic molecules by $CD8^+$ T cells purified from patients with COPD (*13*, *60*, *61*), suggesting that local interactions with cells such as fibrocytes may play a pivotal role in CD8 polarization in COPD. In particular, TNF-α has

proinflammatory and prooxidative actions (*62*), and its overexpression has been associated with emphysema (*63*). TNF-α can directly contribute to cytolysis, together with the cytotoxic granzyme B (*64*) and in synergy with IFN-γ (*65*). TNF-α can also indirectly participate to extracellular matrix degradation through the induction of matrix metalloproteinases (*66*). Simultaneously, the production of the pro-fibrotic IL-17 was also induced upon co-culture with fibrocytes, raising the possibility that the interaction between $CD8^+$ T cells and fibrocyte participates to the generation of IL-17-secreting $CD8^+$ T cells in airways of patients with COPD (*67*). Interestingly, IL-17 is able to simulate matrix components synthesis in other cell types, including fibrocytes, and promotes CD40-mediated IL-6 production by fibrocytes (*68*). Cooperative interactions between fibrocytes and $CD8^+$ T cells, through tissue destruction and abnormal matrix components synthesis, may thus directly contribute to the loss of normal lung function. On the other hand, $CD8^+$ T cell production of anti-inflammatory cytokines such as IL-10, was also stimulated upon co-culture with fibrocytes. In total, rather than the net production of each cytokine, it is probably the balance or imbalance between pro-inflammatory and anti-inflammatory molecules that will dictate the outcome of the inflammatory process.

Whereas the field of respiratory research is rapidly moving towards an exhaustive description of modifications of molecular and cellular components in diseased lungs, the actual transition between a healthy to a diseased state, although critical, remains very difficult to investigate. We developed here a probabilistic cellular automata type model to explore of dynamic behaviors and interactions between fibrocytes and $CD8^+$ T cells. Previous agent-based computational approaches have been used to describe the switch from normal to allergic response (*69*) and airway remodeling in asthma (*70*), but, to our knowledge, this type of modeling was never applied to COPD. Qualitative estimates of

probabilities that govern cell death, proliferation, infiltration and displacement are derived from experimental data from our study and others. We could simulate spatiotemporal behaviors of cells in the lamina propria over long period of time (*i.e.*, 20 years) and we showed that this model can accurately reproduce the absolute and relative repartition of fibrocytes and $CD8^+$ T cells in both control and COPD situations.

Although simulated and *in situ* data were close, the variances of *in silico* data were smaller than the *in situ* measurements, which can be probably explained by the fact that cell diversity and interactions are far more complex that those considered in this model. Nevertheless, it appears that (i) our model captures important aspect of reality, and (ii) modifications of specific cellular processes and local interactions, *i.e.* fibrocyte-induced $CD8^+$ T cell proliferation and fibrocyte attraction towards $CD8^+$ T cells, are sufficient to reproduce the shift of histological composition between the control and COPD situations. This theoretical approach and associated simulations allowed us to validate the key hypothesis of modification of local interactions, and to show that that the specific values of the COPD parameters led to an increased cell density and the spatial patterns observed in patients with COPD. The simulations made it possible to follow over time various quantities of interest and to empirically determine the time when the stationary state is achieved, that would be difficult to reveal in any other way. Given the consistency of our results with those from the literature, our model provides a unique opportunity to decipher the dynamics of increased interactions between the two cell types as well as the infinite possibility to investigate therapeutic strategies.

The present *in vitro* model has limitations, including the use of circulating cells for some *in vitro* experiments and the difficulty in extrapolating results obtained from these assays to in vivo processes. However, we took this limit into account in our modelization approach, by

using a combination of our experiments and measurements obtained in tissues, to accurately determine the dedicated parameters (*42*). Even if computational modelization was done in 2D, whereas the bronchi are 3D structures, we believe that our model is representative as it mimics the cellular distribution of normal and pathological airways, that was also quantified in 2D lung sections. Besides this, some quantitative features of our approach are still valid in 3D, such as the probabilities that govern cell death, proliferation and infiltration, whereas others are expected to change with dimensionality, such as displacement rules.

From our study and others (*71*, *72*), it is now clear that the fate of $CD8^+$ T cells in distal airways may depend on multiple successive interactions with different cell types, including fibrocytes. We believe that targeting interaction between structural and immune cells should be considered in future drug discovery programs and that computational modelization should help to refine drug priority.

Materials and Methods

Study Populations

Lung tissues for the *in situ* study were obtained from a previously described cohort (*6*). Briefly, subjects more than 40 years of age were eligible for enrolment if they required thoracic lobectomy surgery for cancer (pN0), lung transplantation or lung volume reduction. A total of 17 COPD patients with a clinical diagnosis of COPD according to the GOLD guidelines (*73*) and 25 non-COPD subjects ("control subjects") with normal lung function testing (*i.e.*, $FEV_1/FVC > 0.70$) and no chronic symptoms (cough or expectoration) were recruited from the University Hospital of Bordeaux.

Lung tissues for the purification of tissular $CD8^+$ T cells were obtained from a separate cohort of patients. A total of 17 patients with COPD and 23 nonsmokers were prospectively recruited from the University Hospital of Bordeaux, according to the GOLD guidelines (*73*) (Table S7). Fragments of distal parenchyma from all subjects were obtained by either lobectomy or transplantation.

To study fibrocyte- $CD8^+$ T cells interplay *in vitro*, blood samples were obtained from a separate cohort of COPD patients, (*i.e.*, COBRA (Bronchial Obstruction and Asthma Cohort; sponsored by the French National Institute of Health and Medical Research, INSERM), as outpatients in the Clinical Investigation Centre of the University Hospital of Bordeaux (Table S8).

All subjects gave their written informed consent to participate to the studies. The studies received approval from the local or national ethics committees.

Identification of bronchial fibrocytes and $CD8^+$ T cells

Fragments of distal parenchyma were obtained from macroscopically normal lung resection or transplantation material. The samples were embedded in paraffin and sections of 2.5 µm

thick were cut, as described previously (*6*). Sections were deparaffinized through three changes of xylene and through graded alcohols to water. Heat induced antigen retrieval was performed using citrate buffer, pH 6 (Fisher Scientific, Illkirch, France) at 96°C in a Pre-Treatment Module (Agilent, Les Ulis, France). Endogenous peroxidases were blocked for 10 min using hydrogen peroxide treatment (Agilent). Nonspecific binding was minimized by incubating the sections with 4% Goat Serum (Agilent) for 30 min, before CD8 staining, and before the double staining for CD45 and FSP1. First, the sections were stained with rabbit anti-CD8 monoclonal antibody (Fisher Scientific) during 45 min, and then incubated with HRP anti-Mouse (Agilent). Immunoreactivity was detected by using the DAB System (Agilent). Second, the same sections were stained with mouse anti-CD45 monoclonal antibody (BD Biosciences, San Jose, CA) overnight and then with rabbit anti-FSP1 polyclonal antibody (Agilent) during 45 min. They were incubated with Alexa568–conjugated anti-Mouse and with Alexa488–conjugated anti-Rabbit (Fisher Scientific) antibodies. Immunoreactivity was detected by fluorescence for FSP1 and CD45 staining.

The sections were imaged using a slide scanner Nanozoomer 2.0HT with fluorescence imaging module (Hamamatsu Photonics, Massy, France) using objective UPS APO 20X NA 0.75 combined to an additional lens 1.75X, leading to a final magnification of 35X. Virtual slides were acquired with a TDI-3CCD camera. Fluorescent acquisitions were done with a mercury lamp (LX2000 200W - Hamamatsu Photonics) and the set of filters adapted for DAPI, Alexa 488 and Alexa 568. Bright field and fluorescence images where acquired with the NDP-scan software (Hamamatsu) and processed with ImageJ.

Quantification of $CD8^+$ T cells was performed, as described in fig. S1A, C. A color deconvolution plugin was used on brightfield image to isolate the signal corresponding to DAB staining. A binary threshold was applied to this grayscale image, followed by a watershed transformation to the segmented image to separate potential neighboring cells

(fig. S1C). $CD8^+$ T cells were then automatically counted by recording all the positive particles with an area greater than 64 μm^2. This threshold was empirically determined on our images to select positive cells. Quantification of dual positive cells for FSP1 and CD45 was performed, as described in Fig. 1B, D. A binary threshold was applied to fluorescence images corresponding to FSP1 and CD45 stainings. These images were combined using the "AND" function of the Fiji "Image Calculator" to select cells dual positive for FSP1 and CD45 double staining (fig. S1D). This was followed by a watershed transformation to separate potential neighboring cells. These $CD45^+$ $FSP1^+$ cells were then automatically counted by recording all the positive particles with an area greater than 64 μm^2.

Quantification of the density of $CD8^+$ T cells, $FSP1^+$ $CD45^+$ cells and $CD8^+$ T cells in interaction with $CD45^+$ $FSP1^+$ cells

This latter segmented image was then used to quantify $CD8^+$ T cells in interaction with $CD45^+$ $FSP1^+$ cells as described in Fig. 1E: each CD8 positive particle with an area greater than 64 μm^2 was enlarged using the dilatation function (4, 8, 10 and 15 pixels dilatation: used to count the cells respectively less than 1.8, 3.6, 4.5 and 6.8 µm apart). This modified image was combined with the segmented image for dual CD45 FSP1 positive staining using the "AND" function of the Fiji "Image Calculator" to select $CD8^+$ T cells in interaction with $CD45^+$ $FSP1^+$ cells. These interacting cells were automatically counted by recording all the positive particles. The lamina propria contour was manually determined on bright field image and the area was calculated. For distal bronchi, the lumen area was also determined and only bronchi less than 2 mm in diameter were analyzed as described previously (*74*). The densities of $CD8^+$ T cells, $FSP1^+$ $CD45^+$ cells and interacting cells were defined by the ratio between the number of positive cells in the lamina propria divided by lamina propria

area. Tissue area and cell measurements were all performed in a blinded fashion for patients' characteristics.

Quantification of the minimal distances between CD45$^+$ FSP1$^+$ cells and CD8$^+$ T cells

The segmented image produced from the DAB staining image was inverted, and a CD8 distance map was built form the latter image (fig. S1F). As a result, the brighter the pixel, the closer the distance from a CD8$^+$ T cell. Conversely, the darker the pixel, the farther away the distance from a CD8$^+$ T cell. On the binary image produced from FSP1 and CD45 staining images, dual positive cells for FSP1 and CD45 were selected in the lamina propria. Each area corresponding to a FSP1$^+$ CD45$^+$ cell was reported on the CD8 distance map, and the minimal gray value in each area was measured and converted to a distance, allowing to measure the minimal distance between the CD45$^+$ FSP1$^+$ cell and neighboring CD8$^+$ T cells. For each patient, a frequency distribution of all minimal distances (with 7 µm binning) and the mean minimal distance were calculated.

Quantification of cell clusters

On the segmented image with dual CD45 FSP1 positive staining combined with CD8 positive staining, centroids from positive particles located in the lamina propria were connected by a Delaunay triangulation, using a custom freely available ImageJ plugin (*75*) (fig. S3A-C, https://github.com/flevet/Delaunay_clustering_ImageJ). All triangles sharing one edge with the ROI defining the lamina propria were removed (fig. S3C, left panel). On the remaining triangulation a distance threshold, corresponding to the minimal mean distance between fibrocytes and CD8$^+$ T cells (40 µm) was applied, allowing to select the connections with a distance lower than the threshold distance (fig. S3C, right panel). The number of clusters and their composition were then automatically recorded.

673

674 **Fibrocyte and CD8$^+$ T cell purification**

675 Peripheral blood mononuclear cells (PBMCs) were first separated from the whole blood by
676 Ficoll-Hypaque (Eurobio Scientific, Les Ulis, France) density gradient centrifugation. Cells
677 were washed twice in cold PBS containing 0.5% bovine serum albumin (BSA, Sigma-
678 Aldrich, Saint Quentin-Fallavier, France) and 2 mM Ethylene Diamine Tetra-acetic Acid
679 (EDTA, Invitrogen, Cergy Pontoise, France). CD8$^+$ T cells were purified by positive
680 selecting using CD8 microbeads (Miltenyi Biotech, Paris, France). CD8$^+$ T cells were
681 washed in a buffered solution ("CTL-Wash™", Cellular Technology Limited, Bonn,
682 Germany) and resuspended in a serum-free freezing media ("CTL-Cryo™ Medium",
683 Cellular Technology Limited, Bonn, Germany) for cryopreservation of freshly-isolated
684 CD8$^+$ T cells during fibrocyte differentiation. The CD8$^+$ T cells-depleted cell fraction was
685 then depleted from CD3$^+$ cells using CD3 microbeads (Miltenyi Biotec). Cell suspension
686 containing fibrocyte precursors was cultured during at least 14 days to induce fibrocyte
687 differentiation: a total of 2.10^6 cells resuspended in 1 ml DMEM (Fisher Scientific, Illkirch,
688 France), containing 4.5 g/l glucose and glutaMAX, supplemented with 20% fetal calf serum
689 (Biowest, Riverside, USA), penicillin/streptomycin and MEM non-essential amino acid
690 solution (Sigma-Aldrich), was added to each well of a 12 well plate. After one week in
691 culture, fibrocyte differentiation was induced by changing the medium for a serum-free
692 medium. Mediums were changed every 2-3 days.

693

694 **Fibrocyte/CD8$^+$ T cells co-culture assay**

695 One day before co-culture, CD8$^+$ T cells were thawed. A buffer solution previously heated
696 to 37°C (PBS 1X with 0.5% BSA and 2mM EDTA) was added to the cell suspension. CD8$^+$
697 T cells were washed with PBS and resuspended in DMEM supplemented with 8% fetal calf

serum for a final concentration of $0.5.10^6$ cells/mL. $CD8^+$ T cells were either stimulated with a low dose of CD3 antibody (3µg / 10^6 cells) to promote cell survival without stimulating cell proliferation ("non-activated" condition), or stimulated overnight with anti-CD3/CD28 coated microbeads (Fisher Scientific) with a bead-to-cell ratio of 1:1 ("activated" condition). At day 0 (co-culture), these beads were removed, $CD8^+$ T cells were stained with 5 µM CellTrace Violet (Fisher Scientific) in case of proliferation experiments, before being added to fibrocyte cultures ($0.5.10^6$ $CD8^+$ T cells/well). In blocking experiments, the antibodies (Abs) directed against LFA-1 (clone HI111, BioLegend, 1µg/mL), CD54 (clone HA58, eBioscience), CD86 (clone IT2.2, eBioscience, 10µg/mL) or CD44 (clone 82102, Biotechne, 10µg/mL) were used with their respective control Abs, mIgG1 κ (clone MOPC-21, BioLegend), mIgG2b κ (eBM 2b, eBioscience), mIgG2B (133303, Biotechne). In LFA-1 and CD44 blocking experiments as well as in glucocorticoid drugs experiments, $CD8^+$ T cells were preincubated respectively with corresponding Abs, budesonide or fluticasone propionate (10^{-8}M, MedChemExpress) at 37°C for 1h before being added to fibrocytes. In CD54 and CD86 blocking experiments, fibrocytes were preincubated with corresponding Abs at 37°C for 1h before adding $CD8^+$ T cells. For indirect co-culture, $CD8^+$ T cells were cultured in 0.4 µm transwell inserts (Sigma-Aldrich) for 12-well plates.

Live imaging

For time-lapse microscopy, cells were imaged after 2 days of co-culture, at 37°C and with 5% CO_2 on an inverted DMi8 stand microscope (Leica, Microsystems, Wetzlar, Germany) equipped with a Flash 4.0 sCMOS camera (Hamamatsu, Japan). The objective used was a HC PL FL L 20X dry 0.4 NA PH1. The multi-positions were done with a ASI MS-2000-500 motorized stage (Applied Scientific Instrumentation, Eugene, USA). The 37°C/5%CO2

atmosphere was created with an incubator box and an gaz heating system (Pecon GmbH, Erbach, Germany). This system was controlled by MetaMorph software (Molecular Devices, Sunnyvale, USA). Phase contrast images were collected every 2 min for 12h. Image analysis and measurements were performed with the ImageJ software. Using the plugin "Cell counter " of the Fiji software, the number of $CD8^+$ T cells in direct contact with a fibrocyte as well as the number of free $CD8^+$ T cells were manually counted at the beginning of the acquisition and after 12 hours of acquisition. Cell tracking was performed using the "Manual Tracking" plugin of the Fiji software to determine the durations of contacts between tracked $CD8^+$ T cell with fibrocytes and the frequency of contact. A contact was defined manually by a direct interaction between $CD8^+$ T cell and fibrocyte. Five numerical variables were collected to characterize $CD8^+$ T cell dynamic over time. The mean speed corresponded to the track length divided by the time of tracking duration. The mean free speed corresponded the length of the track when the T cell was not interacting with any other cell, divided by the time spent free. The mean contact speed corresponded to the length of the track when the T cell is in contact with a fibrocyte, divided by the time spent in contact. For each T cell and for each contact, a contact time was defined as the time spent in contact until the T cell becomes free again. Then, each T cell can have many contact times with fibrocytes. The contact coefficient was defined by the proportion of time the T cell was in contact with a fibrocyte divided by the time of tracking duration.

$CD8^+$ T cell characterization by flow cytometry

Four or 6 days after co-culture, $CD8^+$ T cells were harvested and manually counted before being processed for FACS analysis. Intracellular cytokines were assessed following stimulation with PMA (25 ng/ml, Sigma-Aldrich), ionomycin (1µM, Sigma-Aldrich) for 4h and brefeldin A (5µg/ml,Sigma-Aldrich) for the last 3 h. Cells were stained with anti-CD8-

PerCP-Vio700, anti-CD45-RA-FITC, and then fixed, permeabilized using the IntraPrep Permeabilization Reagent Kit (Beckman Coulter) and stained with anti-Granzyme-APC, anti-TNF-α-PE, anti-IFN-γ-APC, anti-IL-17- PE-Cy7, anti-IL-10-PE or isotype controls (Miltenyi Biotech, Paris, France). The percentage of cell proliferation was estimated using Cell Trace Violet fluorescence loss. FACS data were acquired using a Canto II 4-Blue 2-Violet 2-Red laser configuration (BD Biosciences). Flow cytometry analysis were performed using Diva 8 (BD Biosciences). Human TNF-α concentration levels were quantified using ELISA following manufacturer's recommendations (BioTechne). Values below the detection limit were counted as zero.

Dataset transcriptomic analysis

The microarray data of tissular $CD8^+$ T cells was downloaded from the Gene Expression Omnibus (http://www.ncbi.nlm.nih.gov/geo/) using a dataset under the accession code GSE61397. Differential expression analysis between patients with COPD and control subjects was performed using the GEO2R interactive web tool. Heatmaps of the expression profiles for genes related to cell adhesion and chemotaxis were visualized with Graphpad Prism 6 software.

Tissular $CD8^+$ T cell purification, culture and secretion profile analyses

After lung parenchyma resection from control or COPD patients, samples were finely chopped at room temperature using scissors and then enzymatically dissociated with 40 IU/mL of collagenase (ThermoFisher) in DMEM medium for 45 min at 37°C. The enzymatic reaction was stopped by adding HBSS medium (Hank's Balanced Salt Solution) without calcium and supplemented with 2mM EDTA (Invitrogen, Cergy Pontoise, France). The cell suspension was filtered twice using 100 µm gauze and 70 µm cell strainer (Fisher

Scientific). Tissular $CD8^+$ T cells were purified by positive selecting using CD8 microbeads (Miltenyi Biotech, Paris, France). Then, tissular $CD8^+$ T cells were resuspended in DMEM supplemented with 8% fetal calf serum, soluble anti-CD3 and anti-CD28 antibodies (respectively 1µg and 3µg for 10^6 cells) for a final concentration of 0.5 x 10^6 cells/mL. After 36h, supernatants from tissular $CD8^+$ T cells were collected and frozen, for migration experiments or for further analyses. Supernatants from different samples obtained either from non-smoking subjects or patients from COPD were pooled for migration experiments. Supernatant concentration of CXCL8 was measured using ELISA (Biotechne). CCL26, CXCL2 and CCL2 concentrations were measured by using a customized Bio-Plex Assay (BioRad, Hercules, CA), using special plate reader (Bio-Plex 200 Systems, BioRad) and software (Bio-Plex manager), according to the manufacturer's instruction.

Fibrocyte migration

Fibrocytes precursors were isolated from peripheral blood as described previously (*5*). Fibrocyte migration was assessed using a modified Boyden chamber assay. The transwell inserts (pore size 8 µm, Dutscher) and the wells were coated for 1h at room temperature with poly-lysine-ethylene glycol (PEG-PLL, SuSoS, Dübendorf, Switzerland) to prevent cell adhesion. A total of 0.3 x 10^6 NANT cells resuspended in 0.2 ml DMEM, containing 4.5 g/l glucose and L-glutamine, supplemented with penicillin/streptomycin and MEM non-essential amino acid solution were added to the upper compartment of each well. When indicated, NANT cells were pretreated for 30 min at 37°C with 200nM reparixin (MedChem Express), an antagonist of CXCR1-2. Supernatants of tissular $CD8^+$ T cells from non-smoking control subjects or COPD patients were added to the bottom compartment of each well. When indicated, supernatants were pretreated for 30 min at 37°C with blocking Ab against CXCL8 (clone 6217, BioTechne, 1µg/mL) or respective control Ab. After 12h, the

content of bottom compartment was removed and DAPI staining was performed to exclude dying cells. Cells were then fixed, permeabilized and stained with anti-Collagen Type I-FITC (Sigma Aldrich), anti-CD45-APC (BD Pharmingen), anti-CXCR1-PE and anti-CXCR2-APC-Cy7 (Miltenyi Biotec, Paris, France). Fibrocyte migration was assessed by flow cytometry using double labeling CD45-Collagen I. To obtain absolute values of migratory cells, flow cytometric counts for each condition were obtained during a constant predetermined time period (1 min). The fraction of migratory fibrocytes was defined as the number $CD45^+$ $Col1^+$ cells counted in the bottom chamber divided by the number of total added cells. These values were normalized to the fraction of migratory fibrocytes obtained in the control condition.

The mathematical model

Exhaustive description of the mathematical model is provided in the supplementary text.

To understand the interaction between fibrocyte and $CD8^+$ T cells in the spatial cellular organization in the peribronchial area, we constructed a discrete time cellular automata model. Two agent types are introduced - $CD8^+$ T cell agents and fibrocytes agents, denoted C and F respectively. C and F cells evolve on a lattice in two-dimensions. We take as surface of interest a zone with a crown shape, containing 3 652 lattice sites corresponding to a total area of approximately 179 000 μm^2, which is in agreement with our in *situ* measurements. Reflecting (zero-flux) boundary conditions are imposed at the external and internal borders. On each site, there is at most one cell. The lattice is initially randomly seeded with both F and C cells at densities corresponding at the mean distribution of non-smokers subjects, reflecting the "healthy" situation : $n_0(C)$ = 660 cells/mm^2, and $n_0(F)$ = 106 cells/mm^2. This corresponds to an average value of $N_0(C)$ =118 C cells and $N_0(F)$ =19 F cells.

We assumed that for a healthy subject as for a patient with COPD, the same model can be applied but with different parameters. These parameters are estimated thanks to experiments and data from the literature (see supplementary text and (*42*) for a complete description, Table S10 for numerical values).

The notations and parameters of the mathematical model are summarized in Table S9 and their numerical values are given in Table S10. We now describe the behavior of the cells and their interactions. F and C cells infiltrate into the peribronchial area at the stable state with the respective probabilities p_{istaF} and p_{istaC}, and during exacerbation, a supplementary infiltration can occur, each year, with the probability p_{iexaF} (resp. p_{iexaC}). In the model, C cells can proliferate with a very low probability p_C, but the presence of F cells in the local neighborhood of a C cell can induce C cell division with increased probability $p_{C/F}$, based on our own results and another study (*21*). We suppose that fibrocytes do not proliferate, as shown by our own *in vitro* observations (data not shown) and other studies (*10*, *34*). F and C cells can move, with probabilities which are determined by the results from chemotaxis experiments (Fig. 2). F and C cells die with a "basal" probability p_{dC} (respectively p_{dF}). C cells also die with an increased probability p_{dC+} when the considered C cell has many other C cells in its neighborhood, in agreement with previous data (*28*). Some of the probabilities are independent of the local environment (p_{istaF}, p_{istaC}, p_{iexaF}, p_{iexaC}, p_C), the other ones being dependent of the local environment ($p_{C/F,}$, p_{dC+} and displacement probabilities) (Fig. 6A).

Each simulation represents a total duration of 20 years and is divided into 3 504 000 iterations, of 3 minutes each. Each type of simulation is performed 160 times. This time period allowed the investigation of COPD development.. At the final state (20 years), the total numbers of F and C cells, the densities of C cells in interaction with F cells, the minimal

distances between C and F cells, and the number and composition of clusters were quantified in the control and COPD situations.

Statistical analyses

Statistical significance, defined as $P < 0.05$, was analyzed by t-tests and MANOVA for variables with parametric distribution, and by Kruskal-Wallis with multiple comparison z tests, Mann-Whitney tests, Wilcoxon tests and Spearman correlation coefficients for variables with non-parametric distribution, with Graphpad Prism 6 software. RStudio software was used to perform stepwise regression and multivariate regression analyses.

References

1. D. M. Mannino, A. S. Buist, Global burden of COPD: risk factors, prevalence, and future trends. *Lancet*. **370**, 765–773 (2007).
2. J. Mead, The Lung's Quiet Zone. *New England Journal of Medicine*. **282**, 1318–1319 (1970).
3. J. C. Hogg, J. Williams, J. B. Richardson, P. T. Macklem, W. M. Thurlbeck, Age as a Factor in the Distribution of Lower-Airway Conductance and in the Pathologic Anatomy of Obstructive Lung Disease. *New England Journal of Medicine*. **282**, 1283–1287 (1970).
4. J.-M. Dayer, How T-lymphocytes are activated and become activators by cell-cell interaction. *European Respiratory Journal*. **22**, 10s–15s (2003).
5. I. Dupin, B. Allard, A. Ozier, E. Maurat, O. Ousova, E. Delbrel, T. Trian, H.-N. Bui, C. Dromer, O. Guisset, E. Blanchard, G. Hilbert, F. Vargas, M. Thumerel, R. Marthan, P.-O. Girodet, P. Berger, Blood fibrocytes are recruited during acute exacerbations of chronic obstructive pulmonary disease through a CXCR4-dependent pathway. *J. Allergy Clin. Immunol.* **137**, 1036-1042.e7 (2016).
6. I. Dupin, M. Thumerel, E. Maurat, F. Coste, E. Eyraud, H. Begueret, T. Trian, M. Montaudon, R. Marthan, P.-O. Girodet, P. Berger, Fibrocyte accumulation in the airway walls of COPD patients. *Eur. Respir. J.* **54** (2019), doi:10.1183/13993003.02173-2018.
7. R. Bucala, L. A. Spiegel, J. Chesney, M. Hogan, A. Cerami, Circulating fibrocytes define a new leukocyte subpopulation that mediates tissue repair. *Mol Med*. **1**, 71–81 (1994).
8. P. Henrot, E. Eyraud, E. Maurat, S. Point, G. Cardouat, J.-F. Quignard, P. Esteves, T. Trian, P.-O. Girodet, R. Marthan, M. Zysman, P. Berger, I. Dupin, Muscarinic receptor M3 activation promotes fibrocytes contraction. *Frontiers in Pharmacology*. **13** (2022) (available at https://www.frontiersin.org/articles/10.3389/fphar.2022.939780).

9. I. Dupin, C. Contin-Bordes, P. Berger, Fibrocytes in Asthma and Chronic Obstructive Pulmonary Disease: Variations on the Same Theme. *Am. J. Respir. Cell Mol. Biol.* **58**, 288–298 (2018).

10. C. Ling, K. Nishimoto, Z. Rolfs, L. M. Smith, B. L. Frey, N. V. Welham, Differentiated fibrocytes assume a functional mesenchymal phenotype with regenerative potential. *Sci Adv*. **5**, eaav7384 (2019).

11. T. C. O'Shaughnessy, T. W. Ansari, N. C. Barnes, P. K. Jeffery, Inflammation in bronchial biopsies of subjects with chronic bronchitis: inverse relationship of CD8+ T lymphocytes with FEV1. *Am J Respir Crit Care Med*. **155**, 852–857 (1997).

12. T. Maeno, A. M. Houghton, P. A. Quintero, S. Grumelli, C. A. Owen, S. D. Shapiro, CD8+ T Cells are required for inflammation and destruction in cigarette smoke-induced emphysema in mice. *J Immunol*. **178**, 8090–8096 (2007).

13. C. M. Freeman, M. K. Han, F. J. Martinez, S. Murray, L. X. Liu, S. W. Chensue, T. J. Polak, J. Sonstein, J. C. Todt, T. M. Ames, D. A. Arenberg, C. A. Meldrum, C. Getty, L. McCloskey, J. L. Curtis, Cytotoxic potential of lung CD8+ T cells increases with COPD severity and with in vitro stimulation by IL-18 or IL-15. *J Immunol*. **184**, 6504–6513 (2010).

14. X. Wang, D. Zhang, A. Higham, S. Wolosianka, X. Gai, L. Zhou, H. Petersen, V. Pinto-Plata, M. Divo, E. K. Silverman, B. Celli, D. Singh, Y. Sun, C. A. Owen, ADAM15 expression is increased in lung CD8+ T cells, macrophages, and bronchial epithelial cells in patients with COPD and is inversely related to airflow obstruction. *Respiratory Research*. **21**, 188 (2020).

15. E. Roos-Engstrand, B. Ekstrand-Hammarström, J. Pourazar, A. F. Behndig, A. Bucht, A. Blomberg, Influence of smoking cessation on airway T lymphocyte subsets in COPD. *COPD*. **6**, 112–120 (2009).

16. J. Wang, R. A. Urbanowicz, P. J. Tighe, I. Todd, J. M. Corne, L. C. Fairclough, Differential activation of killer cells in the circulation and the lung: a study of current smoking status and chronic obstructive pulmonary disease (COPD). *PLoS One*. **8**, e58556 (2013).

17. J.-S. Zhou, Z.-Y. Li, X.-C. Xu, Y. Zhao, Y. Wang, H.-P. Chen, M. Zhang, Y.-F. Wu, T.-W. Lai, C.-H. Di, L.-L. Dong, J. Liu, N.-X. Xuan, C. Zhu, Y.-P. Wu, H.-Q. Huang, F.-G. Yan, W. Hua, Y. Wang, W.-N. Xiong, H. Qiu, T. Chen, D. Weng, H.-P. Li, X. Zhou, L. Wang, F. Liu, X. Lin, S.-M. Ying, W. Li, M. Imamura, M. E. Choi, M. R. Stampfli, A. M. K. Choi, Z.-H. Chen, H.-H. Shen, Cigarette smoke-initiated autoimmunity facilitates sensitisation to elastin-induced COPD-like pathologies in mice. *European Respiratory Journal*. **56** (2020), doi:10.1183/13993003.00404-2020.

18. M. C. Morissette, J. Parent, J. Milot, Perforin, granzyme B, and FasL expression by peripheral blood T lymphocytes in emphysema. *Respiratory Research*. **8**, 62 (2007).

19. R. T. McKendry, C. M. Spalluto, H. Burke, B. Nicholas, D. Cellura, A. Al-Shamkhani, K. J. Staples, T. M. A. Wilkinson, Dysregulation of Antiviral Function of CD8+ T Cells in the Chronic Obstructive Pulmonary Disease Lung. Role of the PD-1–PD-L1 Axis. *Am J Respir Crit Care Med*. **193**, 642–651 (2016).

20. S. Grundy, J. Plumb, S. Lea, M. Kaur, D. Ray, D. Singh, Down regulation of T cell receptor expression in COPD pulmonary CD8 cells. *PLoS One*. **8**, e71629 (2013).

21. T. Afroj, A. Mitsuhashi, H. Ogino, A. Saijo, K. Otsuka, H. Yoneda, M. Tobiume, N. T. Nguyen, H. Goto, K. Koyama, M. Sugimoto, O. Kondoh, H. Nokihara, Y. Nishioka, Blockade of

926 PD-1/PD-L1 Pathway Enhances the Antigen-Presenting Capacity of Fibrocytes. *J Immunol* (2021),
927 doi:10.4049/jimmunol.2000909.
928 22. M. Saetta, A. Di STEFANO, G. Turato, F. M. Facchini, L. Corbino, C. E. Mapp, P.
929 Maestrelli, A. Ciaccia, L. M. Fabbri, CD8+ T-Lymphocytes in Peripheral Airways of Smokers with
930 Chronic Obstructive Pulmonary Disease. *Am J Respir Crit Care Med*. **157**, 822–826 (1998).
931 23. P. Hombrink, C. Helbig, R. A. Backer, B. Piet, A. E. Oja, R. Stark, G. Brasser, A. Jongejan,
932 R. E. Jonkers, B. Nota, O. Basak, H. C. Clevers, P. D. Moerland, D. Amsen, R. A. W. van Lier,
933 Programs for the persistence, vigilance and control of human CD8+ lung-resident memory T cells.
934 *Nat Immunol*. **17**, 1467–1478 (2016).
935 24. R. Bertini, M. Allegretti, C. Bizzarri, A. Moriconi, M. Locati, G. Zampella, M. N.
936 Cervellera, V. Di Cioccio, M. C. Cesta, E. Galliera, F. O. Martinez, R. Di Bitondo, G. Troiani, V.
937 Sabbatini, G. D'Anniballe, R. Anacardio, J. C. Cutrin, B. Cavalieri, F. Mainiero, R. Strippoli, P.
938 Villa, M. Di Girolamo, F. Martin, M. Gentile, A. Santoni, D. Corda, G. Poli, A. Mantovani, P.
939 Ghezzi, F. Colotta, Noncompetitive allosteric inhibitors of the inflammatory chemokine receptors
940 CXCR1 and CXCR2: prevention of reperfusion injury. *Proc Natl Acad Sci U S A*. **101**, 11791–
941 11796 (2004).
942 25. R. Obst, The Timing of T Cell Priming and Cycling. *Frontiers in Immunology*. **6** (2015)
943 (available at https://www.frontiersin.org/article/10.3389/fimmu.2015.00563).
944 26. C. Balmelli, N. Ruggli, K. McCullough, A. Summerfield, Fibrocytes are potent stimulators
945 of anti-virus cytotoxic T cells. *J Leukoc Biol*. **77**, 923–933 (2005).
946 27. L. Bianchetti, M. Barczyk, J. Cardoso, M. Schmidt, A. Bellini, S. Mattoli, Extracellular
947 matrix remodelling properties of human fibrocytes. *J Cell Mol Med*. **16**, 483–495 (2012).
948 28. S. Zenke, M. M. Palm, J. Braun, A. Gavrilov, P. Meiser, J. P. Böttcher, N. Beyersdorf, S.
949 Ehl, A. Gerard, T. Lämmermann, T. N. Schumacher, J. B. Beltman, J. C. Rohr, Quorum Regulation
950 via Nested Antagonistic Feedback Circuits Mediated by the Receptors CD28 and CTLA-4 Confers
951 Robustness to T Cell Population Dynamics. *Immunity*. **52**, 313-327.e7 (2020).
952 29. P. Mrass, S. R. Oruganti, G. M. Fricke, J. Tafoya, J. R. Byrum, L. Yang, S. L. Hamilton,
953 M. J. Miller, M. E. Moses, J. L. Cannon, ROCK regulates the intermittent mode of interstitial T cell
954 migration in inflamed lungs. *Nat Commun*. **8**, 1010 (2017).
955 30. S. R. McMaster, J. J. Wilson, H. Wang, J. E. Kohlmeier, Airway-Resident Memory CD8 T
956 Cells Provide Antigen-Specific Protection against Respiratory Virus Challenge through Rapid IFN-
957 γ Production. *J Immunol*. **195**, 203–209 (2015).
958 31. L. Siena, M. Gjomarkaj, J. Elliot, E. Pace, A. Bruno, S. Baraldo, M. Saetta, M. R.
959 Bonsignore, A. James, Reduced apoptosis of CD8+ T-lymphocytes in the airways of smokers with
960 mild/moderate COPD. *Respir Med*. **105**, 1491–1500 (2011).
961 32. J. G. Gribben, G. J. Freeman, V. A. Boussiotis, P. Rennert, C. L. Jellis, E. Greenfield, M.
962 Barber, V. A. Restivo, X. Ke, G. S. Gray, CTLA4 mediates antigen-specific apoptosis of human T
963 cells. *PNAS*. **92**, 811–815 (1995).
964 33. P. Scheipers, H. Reiser, Fas-independent death of activated CD4+ T lymphocytes induced
965 by CTLA-4 crosslinking. *PNAS*. **95**, 10083–10088 (1998).
966 34. M. Schmidt, G. Sun, M. A. Stacey, L. Mori, S. Mattoli, Identification of circulating
967 fibrocytes as precursors of bronchial myofibroblasts in asthma. *J Immunol*. **171**, 380–389 (2003).

35. M. Bivas-Benita, G. O. Gillard, L. Bar, K. A. White, R. J. Webby, A.-H. Hovav, N. L. Letvin, Airway CD8 + T cells induced by pulmonary DNA immunization mediate protective anti-viral immunity. *Mucosal Immunology*. **6**, 156–166 (2013).

36. J. Schyns, Q. Bai, C. Ruscitti, C. Radermecker, S. De Schepper, S. Chakarov, F. Farnir, D. Pirottin, F. Ginhoux, G. Boeckxstaens, F. Bureau, T. Marichal, Non-classical tissue monocytes and two functionally distinct populations of interstitial macrophages populate the mouse lung. *Nat Commun*. **10**, 3964 (2019).

37. J. R. Hurst, J. Vestbo, A. Anzueto, N. Locantore, H. Müllerova, R. Tal-Singer, B. Miller, D. A. Lomas, A. Agusti, W. Macnee, P. Calverley, S. Rennard, E. F. M. Wouters, J. A. Wedzicha, Evaluation of COPD Longitudinally to Identify Predictive Surrogate Endpoints (ECLIPSE) Investigators, Susceptibility to exacerbation in chronic obstructive pulmonary disease. *N Engl J Med*. **363**, 1128–1138 (2010).

38. K. H. Ely, T. Cookenham, A. D. Roberts, D. L. Woodland, Memory T cell populations in the lung airways are maintained by continual recruitment. *J. Immunol.* **176**, 537–543 (2006).

39. S. Takamura, H. Yagi, Y. Hakata, C. Motozono, S. R. McMaster, T. Masumoto, M. Fujisawa, T. Chikaishi, J. Komeda, J. Itoh, M. Umemura, A. Kyusai, M. Tomura, T. Nakayama, D. L. Woodland, J. E. Kohlmeier, M. Miyazawa, Specific niches for lung-resident memory CD8+ T cells at the site of tissue regeneration enable CD69-independent maintenance. *J Exp Med*. **213**, 3057–3073 (2016).

40. C. M. Freeman, J. L. Curtis, S. W. Chensue, CC chemokine receptor 5 and CXC chemokine receptor 6 expression by lung CD8+ cells correlates with chronic obstructive pulmonary disease severity. *Am J Pathol*. **171**, 767–776 (2007).

41. M. Saetta, S. Baraldo, L. Corbino, G. Turato, F. Braccioni, F. Rea, G. Cavallesco, G. Tropeano, C. E. Mapp, P. Maestrelli, A. Ciaccia, L. M. Fabbri, CD8+ve cells in the lungs of smokers with chronic obstructive pulmonary disease. *Am J Respir Crit Care Med*. **160**, 711–717 (1999).

42. I. Dupin, E. Eyraud, É. Maurat, J.-M. Sac-Épée, P. Vallois, Probabilistic Cellular Automata modeling of intercellular interactions in airways: complex pattern formation in patients with Chronic Obstructive Pulmonary Disease (2022), (available at https://hal.archives-ouvertes.fr/hal-03572045).

43. A. Løkke, P. Lange, H. Scharling, P. Fabricius, J. Vestbo, Developing COPD: a 25 year follow up study of the general population. *Thorax*. **61**, 935–939 (2006).

44. F. Xu, D. M. Vasilescu, D. Kinose, N. Tanabe, K. W. Ng, H. O. Coxson, J. D. Cooper, T.-L. Hackett, S. E. Verleden, B. M. Vanaudenaerde, C. S. Stevenson, M. E. Lenburg, A. Spira, W. C. Tan, D. D. Sin, R. T. Ng, J. C. Hogg, The molecular and cellular mechanisms associated with the destruction of terminal bronchioles in chronic obstructive pulmonary disease. *European Respiratory Journal* (2021), doi:10.1183/13993003.01411-2021.

45. V. N. Ngo, H. L. Tang, J. G. Cyster, Epstein-Barr virus-induced molecule 1 ligand chemokine is expressed by dendritic cells in lymphoid tissues and strongly attracts naive T cells and activated B cells. *J. Exp. Med.* **188**, 181–191 (1998).

46. U. H. von Andrian, C. R. Mackay, T-cell function and migration. Two sides of the same coin. *N. Engl. J. Med.* **343**, 1020–1034 (2000).

47. C. R. Mackay, Chemokines: immunology's high impact factors. *Nat. Immunol.* **2**, 95–101 (2001).

48. M. J. Miller, A. S. Hejazi, S. H. Wei, M. D. Cahalan, I. Parker, T cell repertoire scanning is promoted by dynamic dendritic cell behavior and random T cell motility in the lymph node. *Proc. Natl. Acad. Sci. U.S.A.* **101**, 998–1003 (2004).

49. P. Henrot, R. Prevel, P. Berger, I. Dupin, Chemokines in COPD: From Implication to Therapeutic Use. *Int J Mol Sci*. **20** (2019), doi:10.3390/ijms20112785.

50. T. M. Conlon, G. John-Schuster, D. Heide, D. Pfister, M. Lehmann, Y. Hu, Z. Ertüz, M. A. Lopez, M. Ansari, M. Strunz, C. Mayr, I. Angelidis, C. Ciminieri, R. Costa, M. S. Kohlhepp, A. Guillot, G. Günes, A. Jeridi, M. C. Funk, G. Beroshvili, S. Prokosch, J. Hetzer, S. E. Verleden, H. Alsafadi, M. Lindner, G. Burgstaller, L. Becker, M. Irmler, M. Dudek, J. Janzen, E. Goffin, R. Gosens, P. Knolle, B. Pirotte, T. Stoeger, J. Beckers, D. Wagner, I. Singh, F. J. Theis, M. H. de Angelis, T. O'Connor, F. Tacke, M. Boutros, E. Dejardin, O. Eickelberg, H. B. Schiller, M. Königshoff, M. Heikenwalder, A. Ö. Yildirim, Inhibition of LTβR signalling activates WNT-induced regeneration in lung. *Nature*. **588**, 151–156 (2020).

51. J. A. Nemzek, C. Fry, B. B. Moore, Adoptive transfer of fibrocytes enhances splenic T-cell numbers and survival in septic peritonitis. *Shock*. **40**, 106–114 (2013).

52. M. L. Dustin, T-cell activation through immunological synapses and kinapses. *Immunol Rev*. **221**, 77–89 (2008).

53. H. D. Moreau, F. Lemaître, E. Terriac, G. Azar, M. Piel, A.-M. Lennon-Dumenil, P. Bousso, Dynamic in situ cytometry uncovers T cell receptor signaling during immunological synapses and kinapses in vivo. *Immunity*. **37**, 351–363 (2012).

54. M. Kaur, L. J. Smyth, P. Cadden, S. Grundy, D. Ray, J. Plumb, D. Singh, T lymphocyte insensitivity to corticosteroids in chronic obstructive pulmonary disease. *Respir Res*. **13**, 20 (2012).

55. P. Henrot, F. Beaufils, M. Thumerel, E. Eyraud, A. Boudoussier, H. Begueret, E. Maurat, P.-O. Girodet, R. Marthan, P. Berger, I. Dupin, M. Zysman, Circulating fibrocytes as a new tool to predict lung cancer progression after surgery? *Eur Respir J*, 2101221 (2021).

56. R. A. Backer, P. Hombrink, C. Helbig, D. Amsen, The Fate Choice Between Effector and Memory T Cell Lineages: Asymmetry, Signal Integration, and Feedback to Create Bistability. *Adv Immunol*. **137**, 43–82 (2018).

57. J. T. Chang, V. R. Palanivel, I. Kinjyo, F. Schambach, A. M. Intlekofer, A. Banerjee, S. A. Longworth, K. E. Vinup, P. Mrass, J. Oliaro, N. Killeen, J. S. Orange, S. M. Russell, W. Weninger, S. L. Reiner, Asymmetric T lymphocyte division in the initiation of adaptive immune responses. *Science*. **315**, 1687–1691 (2007).

58. G. Chrysofakis, N. Tzanakis, D. Kyriakoy, M. Tsoumakidou, I. Tsiligianni, M. Klimathianaki, N. M. Siafakas, Perforin expression and cytotoxic activity of sputum CD8+ lymphocytes in patients with COPD. *Chest*. **125**, 71–76 (2004).

59. P. J. Barnes, Inflammatory mechanisms in patients with chronic obstructive pulmonary disease. *J Allergy Clin Immunol*. **138**, 16–27 (2016).

60. G. Hodge, J. Nairn, M. Holmes, P. N. Reynolds, S. Hodge, Increased intracellular T helper 1 proinflammatory cytokine production in peripheral blood, bronchoalveolar lavage and intraepithelial T cells of COPD subjects. *Clin Exp Immunol*. **150**, 22–29 (2007).

61. M. W. Lethbridge, D. M. Kemeny, J. C. Ratoff, B. J. O'Connor, C. M. Hawrylowicz, C. J. Corrigan, A novel technique to explore the functions of bronchial mucosal T cells in chronic obstructive pulmonary disease: application to cytotoxicity and cytokine immunoreactivity. *Clin Exp Immunol*. **161**, 560–569 (2010).

62. S. Mukhopadhyay, J. R. Hoidal, T. K. Mukherjee, Role of TNFalpha in pulmonary pathophysiology. *Respir Res*. **7**, 125 (2006).

63. L. K. A. Lundblad, J. Thompson-Figueroa, T. Leclair, M. J. Sullivan, M. E. Poynter, C. G. Irvin, J. H. T. Bates, Tumor Necrosis Factor–α Overexpression in Lung Disease. *Am J Respir Crit Care Med*. **171**, 1363–1370 (2005).

64. F. Velotti, I. Barchetta, F. A. Cimini, M. G. Cavallo, Granzyme B in Inflammatory Diseases: Apoptosis, Inflammation, Extracellular Matrix Remodeling, Epithelial-to-Mesenchymal Transition and Fibrosis. *Front Immunol*. **11**, 587581 (2020).

65. B. D. Williamson, E. A. Carswell, B. Y. Rubin, J. S. Prendergast, L. J. Old, Human tumor necrosis factor produced by human B-cell lines: synergistic cytotoxic interaction with human interferon. *PNAS*. **80**, 5397–5401 (1983).

66. J. L. Wright, H. Tai, R. Wang, X. Wang, A. Churg, Cigarette smoke upregulates pulmonary vascular matrix metalloproteinases via TNF-alpha signaling. *Am J Physiol Lung Cell Mol Physiol*. **292**, L125-133 (2007).

67. Y. Chang, J. Nadigel, N. Boulais, J. Bourbeau, F. Maltais, D. H. Eidelman, Q. Hamid, CD8 positive T cells express IL-17 in patients with chronic obstructive pulmonary disease. *Respiratory Research*. **12**, 43 (2011).

68. H. Hayashi, A. Kawakita, S. Okazaki, M. Yasutomi, H. Murai, Y. Ohshima, IL-17A/F modulates fibrocyte functions in cooperation with CD40-mediated signaling. *Inflammation*. **36**, 830–838 (2013).

69. J. J. Pothen, M. E. Poynter, J. H. T. Bates, A computational model of unresolved allergic inflammation in chronic asthma. *Am J Physiol Lung Cell Mol Physiol*. **308**, L384–L390 (2015).

70. R. Saunders, H. Kaul, R. Berair, S. Gonem, A. Singapuri, A. J. Sutcliffe, L. Chachi, M. S. Biddle, D. Kaur, M. Bourne, I. D. Pavord, A. J. Wardlaw, S. H. Siddiqui, R. A. Kay, B. S. Brook, R. H. Smallwood, C. E. Brightling, DP2 antagonism reduces airway smooth muscle mass in asthma by decreasing eosinophilia and myofibroblast recruitment. *Sci Transl Med*. **11** (2019), doi:10.1126/scitranslmed.aao6451.

71. S. Takamura, S. Kato, C. Motozono, T. Shimaoka, S. Ueha, K. Matsuo, K. Miyauchi, T. Masumoto, A. Katsushima, T. Nakayama, M. Tomura, K. Matsushima, M. Kubo, M. Miyazawa, Interstitial-resident memory CD8+ T cells sustain frontline epithelial memory in the lung. *Journal of Experimental Medicine*. **216**, 2736–2747 (2019).

72. M. M. Hufford, T. S. Kim, J. Sun, T. J. Braciale, Antiviral CD8+ T cell effector activities in situ are regulated by target cell type. *J Exp Med*. **208**, 167–180 (2011).

73. Global Initiative for Chronic Obstructive Lung Disease (GOLD). Global Strategy for the Diagnosis, Management, and Prevention of Chronic Obstructive Pulmonary Disease. GOLD, 2022. Available from: https://goldcopd.org/2022-gold-reports-2/
Date last accessed:October 1, 2022.

74. J. C. Hogg, F. Chu, S. Utokaparch, R. Woods, W. M. Elliott, L. Buzatu, R. M. Cherniack, R. M. Rogers, F. C. Sciurba, H. O. Coxson, P. D. Paré, The nature of small-airway obstruction in chronic obstructive pulmonary disease. *N Engl J Med*. **350**, 2645–2653 (2004).

75. C. A. Schneider, W. S. Rasband, K. W. Eliceiri, NIH Image to ImageJ: 25 years of image analysis. *Nat Methods*. **9**, 671–675 (2012).

76. M. Hasegawa, Y. Nasuhara, Y. Onodera, H. Makita, K. Nagai, S. Fuke, Y. Ito, T. Betsuyaku, M. Nishimura, Airflow Limitation and Airway Dimensions in Chronic Obstructive Pulmonary Disease. *Am J Respir Crit Care Med*. **173**, 1309–1315 (2006).

77. P. Hombrink, C. Helbig, R. A. Backer, B. Piet, A. E. Oja, R. Stark, G. Brasser, A. Jongejan, R. E. Jonkers, B. Nota, O. Basak, H. C. Clevers, P. D. Moerland, D. Amsen, R. A. W. van Lier, Programs for the persistence, vigilance and control of human CD8+ lung-resident memory T cells. *Nat. Immunol.* **17**, 1467–1478 (2016).

78. L. Antonioli, C. Blandizzi, P. Pacher, M. Guilliams, G. Haskó, Quorum sensing in the immune system. *Nat Rev Immunol*. **18**, 537–538 (2018).

Acknowledgments

We thank the study participants and the staff of the Thoracic Surgery, Radiology, Pathology, Respiratory, Lung Function Testing departments from the University Hospital of Bordeaux (Bordeaux, France), Isabelle Goasdoue, Isabelle Bernis, Natacha Robert, Virginie Niel, and Marine Servat from the clinical investigation center for technical assistance, and Atika Zouine and Vincent Pitard for technical assistance at the Flow cytometry facility (CNRS UMS 3427, INSERM US 005, Univ. Bordeaux, F-33000 Bordeaux, France), Christel Poujol, Sébastien Marais and Fabrice Cordelières for help with imaging and image analysis et the Bordeaux Imaging Centre (BIC; Bordeaux, France). Microscopy was performed at BIC, a service unit of the CNRS-INSERM and Bordeaux University, a member of the national BioImaging infrastructure of France supported by the French National Research Agency (ANR-10-INBS-04).

Funding: The project was funded by :

the “Fondation de l’Université de Bordeaux” (Fonds pour les maladies chroniques nécessitant une assistance médico-technique FGLMR/AVAD) (ID)

the “Agence Nationale de la Recherche” (ANR-21-CE18-0001-01) (ID)

AstraZeneca (an unrestricted grant to PB).

The COBRA cohort was funded by AstraZeneca, Chiesi, Glaxo-SmithKline, Novartis and Roche.

Author contributions:

Conceptualization: PV, CCB, PB, ID
Methodology: EE, EM, PH, MZ, HB, POG, MT, RHC, FL, PV, CCB, PB, ID
Software: JMSE, PV, FL
Formal analysis: EE, EM, JMSE, PV, ID
Investigation: EE, EM, JMSE, PH, MZ, PE, TT, MT, RHC, PV, CCB, ID
Visualization: EE, EM, JMSE, PH, ID
Supervision: ID
Writing—original draft: EE, ID

Writing—review & editing: EE, PH, RM, PV, CCB, PB, ID

Competing interests: PB, POG, ID have a patent (EP N°3050574: Use of plerixafor for treating and/or preventing acute exacerbations of chronic obstructive pulmonary disease) granted.
MZ reports grants from AstraZeneca ; grants “Fondation Bordeaux Université,” with funding from "Assistance Ventilatoire à Domicile" (AVAD) and "Fédération Girondine de Lutte contre les Maladies Respiratoires" (FGLMR) and personal fees from AstraZeneca, Boehringer Ingelheim, Novartis, Chiesi, GlaxoSmithKline and non-financial support Lilly outside the submitted work;
POG reports grants, personal fees and non-financial support from AstraZeneca, personal fees and non-financial support from Chiesi, personal fees and non-financial support from GlaxoSmithKline, personal fees and non-financial support from Novartis, personal fees and non-financial support from Sanofi, outside the submitted work;
PB reports grants from AstraZeneca, Glaxo-Smith-Kline, Novartis, Chiesi, which support COBRA during the conduct of the study; grants and personal fees from AstraZeneca, BoehringerIngelheim, Novartis, personal fees and non-financial support from Chiesi, Sanofi, Menarini, outside the submitted work;
ID and PH report grants from the “Fondation Bordeaux Université,” with funding from "Assistance Ventilatoire à Domicile" (AVAD) and "Fédération Girondine de Lutte contre les Maladies Respiratoires" (FGLMR) during the conduct of the study.

All other authors declare they have no competing interests.

Data and materials availability: All data needed to evaluate the conclusions are present in the paper, the Supplementary Materials, and/or the deposited data. The customized ImageJ plugin used to perform Delaunay triangulation and cluster quantification is available here:
https://github.com/flevet/Delaunay_clustering_ImageJ
A complete version of the code for launching the simulations associated to control and COPD dynamics can be downloaded from the following site: https://plmbox.math.cnrs.fr/d/49bcbc1db63a4654be7e/

Figures

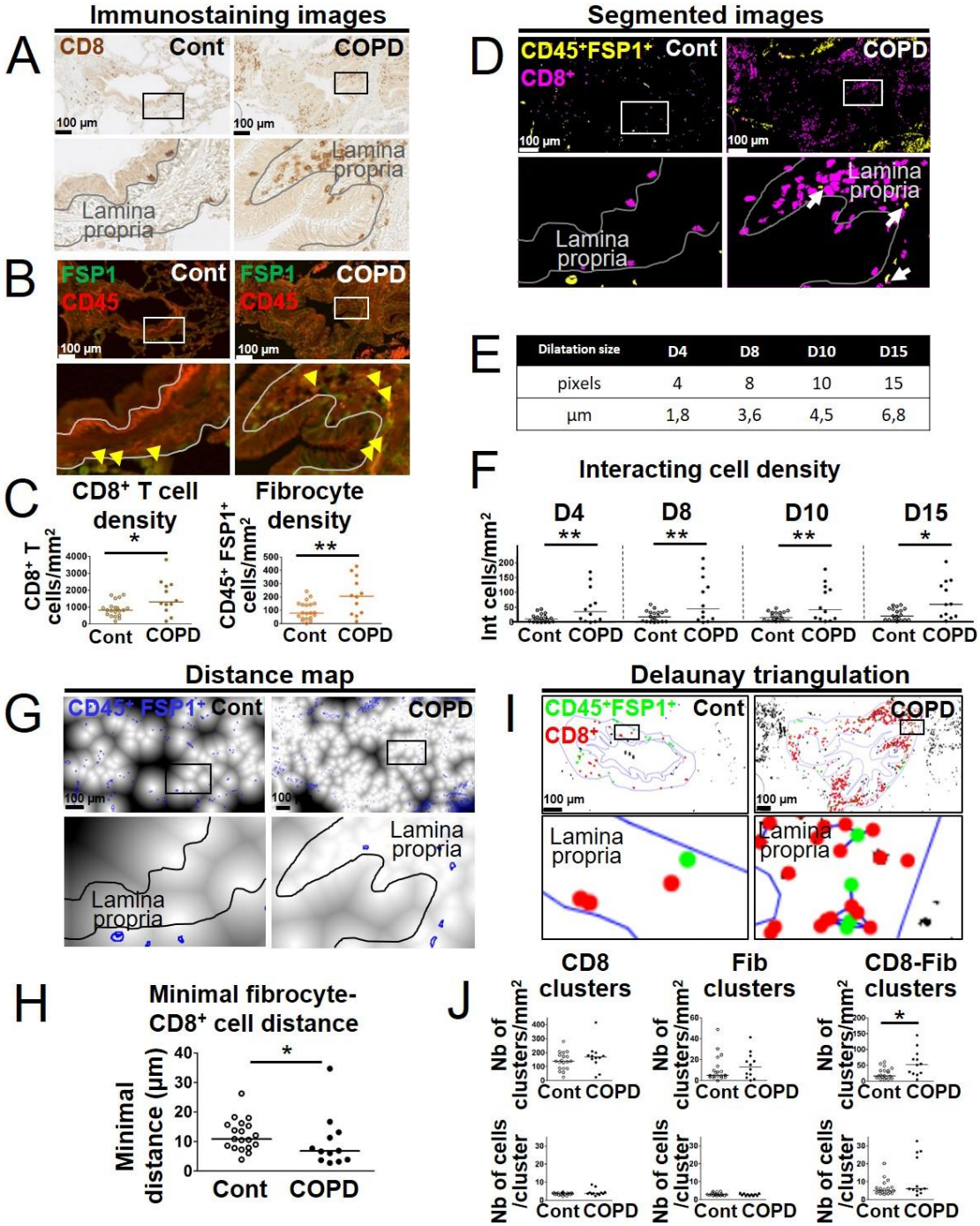

Fig. 1. Increased interactions between CD8⁺ T cells, CD45⁺ FSP1⁺ cells in distal airways of COPD patients. (A, B) Representative stainings of CD8 (brown, **A**), CD45 (red, **B**) and FSP1 (green, **B**) in distal bronchial tissue specimens from a control subject (left) and a COPD patient (right). The yellow arrowheads indicate fibrocytes, defined as CD45⁺ FSP1⁺ cells. (**C**) Quantification of CD8⁺ T cells and fibrocyte densities (normalized by the sub-epithelial area) in one specimen/patient. (**D**) Merged segmented images for CD8 and CD45-FSP1 staining, showing CD8⁺ T cells and CD45⁺ FSP1⁺ cells respectively in magenta and yellow. The white arrows indicate interacting cells, detected by dilatation of CD8 positive particle. (**E**) Table showing the correspondence between dilatations in pixels and µm. F, Quantification of interacting cells densities (normalized by the sub-epithelial area) in one

specimen/patient, using the different dilatations sizes (**E**). (**G**) Distance maps built from the binary image produced from CD8 staining, with $FSP1^+$ $CD45^+$ cells (blue outlines). (**H**) Quantification of the mean minimal distances between fibrocyte and $CD8^+$ T cells in one specimen/patient. (**I**) Cluster analysis performed by Delaunay triangulation on segmented images for CD8 and CD45-FSP1 staining, followed by the application of a threshold value (40 μm) above which connections are not kept. $CD8^+$ T cells and fibrocytes appear respectively with green and red dots, connections are shown in blue. (**J**) First row: densities of clusters containing exclusively $CD8^+$ T cells ("CD8 clusters"), fibrocytes ("Fib clusters") and both cell types ("CD8-Fib clusters") normalized by the sub-epithelial area) in one specimen/patient. Second row: mean number of cells by cluster. (**C, F, H, J**) The medians are represented as horizontal lines. *: $P<0.05$, **:$P<0.01$; ***: $P<0.001$. unpaired t-tests or Mann Whitney tests.

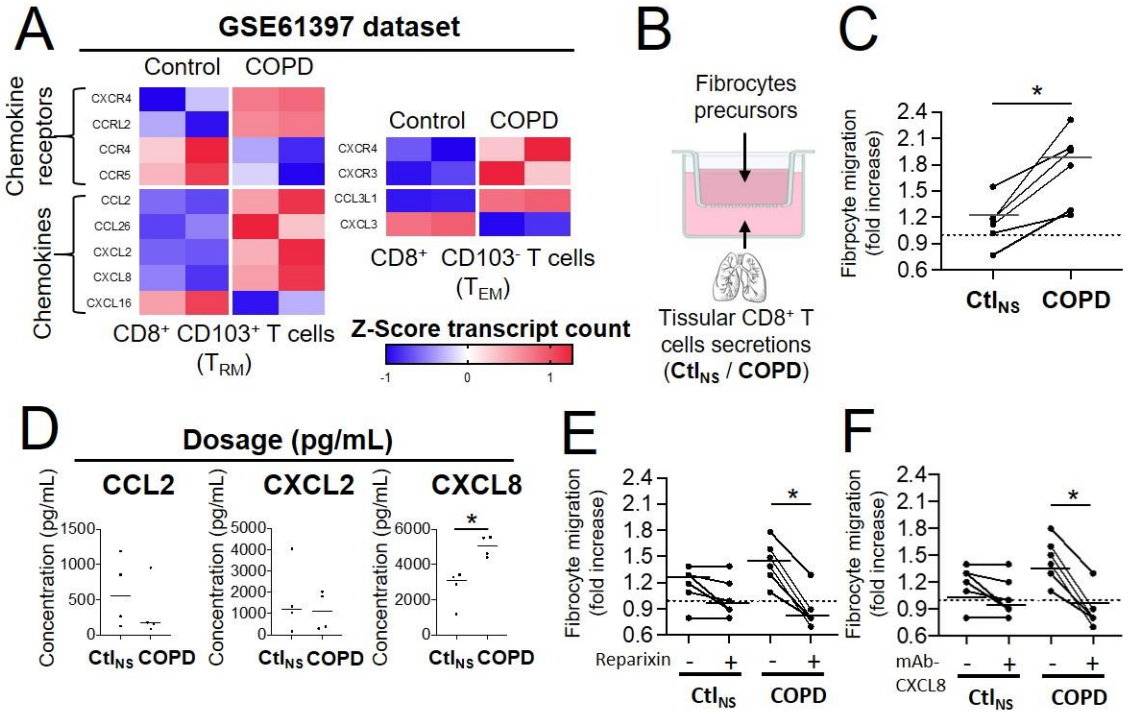

Fig. 2. CD8$^+$ T cells from COPD tissue have increased chemoattractive properties for fibrocytes. (A) Heatmaps showing the expression of differentially expressed genes with p-value<0.05 of chemokines and chemokine receptors in resting tissular tissue resident memory T-cells (T_{RM}) and effector memory T-cells (T_{EM}) from patients with COPD (n=2 independent samples) in comparison with control subjects (n=2 independent samples) (GEO accession GSE61397). Expression values are expressed as Z-score transformed transcript count. (**B**) Migration experiment design. (**C**) Migration of fibrocytes from patients with COPD in response to CD8$^+$ T cells supernatants from control subjects (Ctl_{NS}) or COPD patients (COPD). (**D**) CCL2, CXCL2 and CXCL8 levels in CD8$^+$ T cells supernatants from non-smoking control subjects (Ctl_{NS}) or patients with COPD (COPD) using BioPlex (CCL2, CXCL2) or ELISA (CXCL8). * P < 0.05, Mann–Whitney test. (**E-F**), Migration of fibrocytes from patients with COPD in response to CD8$^+$ T cells supernatants from control subjects (Ctl_{NS}) or COPD patients (COPD), in the presence of 200nM Reparixin (+) or corresponding vehicle (-) (**E**), and in the presence of 1µg/mL blocking antibody for CXCL8 (+) or control antibody (-) (**F**). * P < 0.05, Wilcoxon matched pairs test.

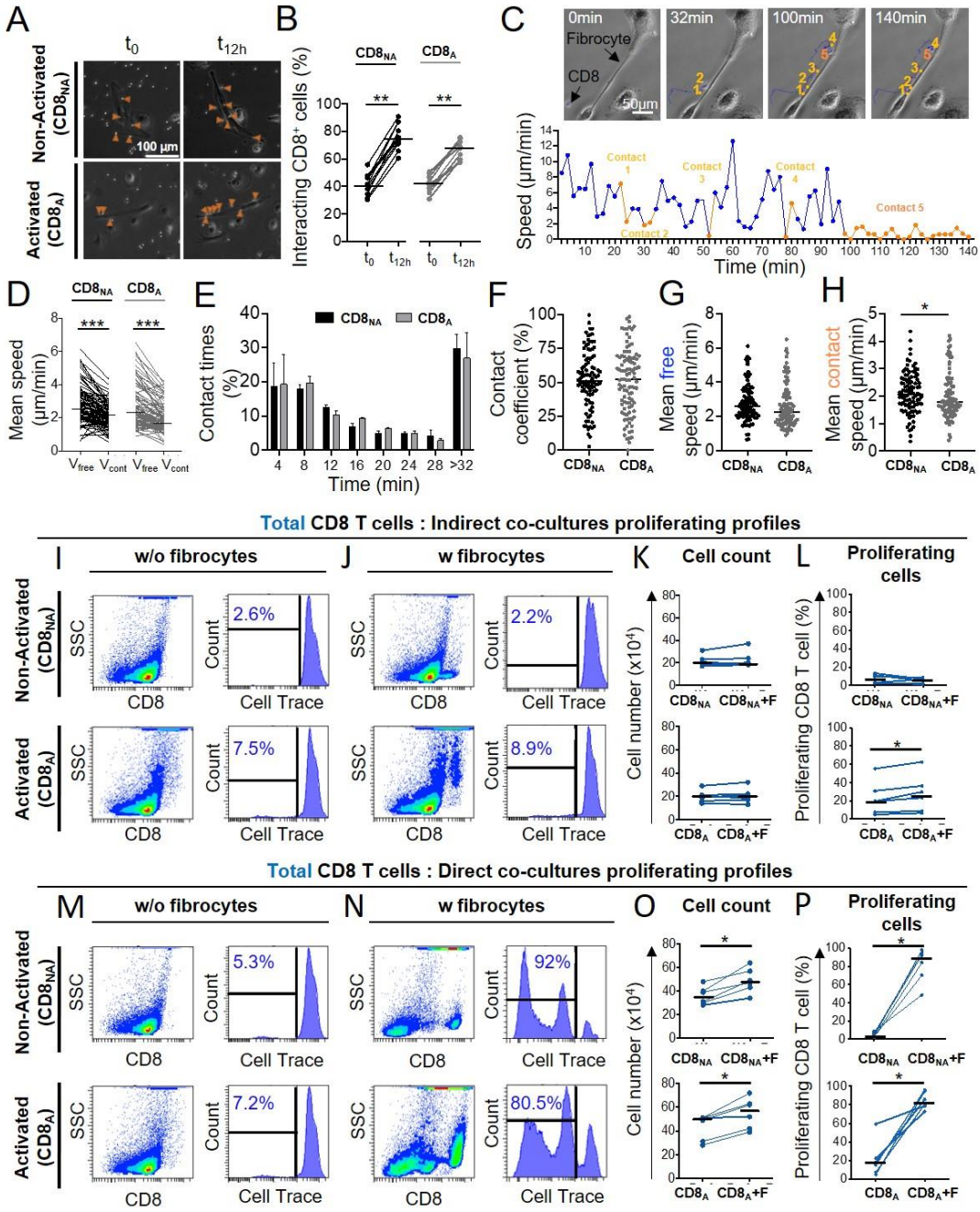

Fig. 3. CD8⁺ T cell repeatedly contact fibrocytes and this contact greatly enhances CD8⁺ T cell proliferation. Prior to co-culture, CD8⁺ T cells have been either non-activated ("$CD8_{NA}$") or activated ("$CD8_A$"). **(A)** Representative brightfield images of co-culture between CD8⁺ T cells and fibrocytes at the initial state of the acquisition (t_0) and after 12 hours (t_{12h}) in both conditions of activation. The orange arrowheads indicate CD8⁺ T cells (bright round-shaped cells) in contact with fibrocytes (elongated adherent cells). (**B**) Quantifications of the proportion of fibrocyte-interacting CD8⁺ T cells at t_0 and t_{12h} in both conditions of activation. (**C**) Top panel: typical CD8⁺ T cells trajectory (blue) relatively to a fibrocyte (elongated adherent cell) for a period of 140 min. Bottom panel: speed (µm/min) over time for the tracked CD8⁺ T cell. Short-lived (<12 min, n=4) and longer-lived (>32 min, n=1) contacts are represented respectively in light and dark orange. (**D**) Comparison of the mean speed of individual CD8⁺ T cells measured in the absence ("V_{free}") or presence ("V_{cont}") of contact with fibrocytes in both conditions of activation. (**E**) Mean frequency

distributions of contact time duration (with 4 min binning) between $CD8^+$ T cells and fibrocytes for $CD8_{NA}$ (black) and $CD8_A$ (gray). Error bars indicate standard error of the mean. (**F**-**H**) Dot plots representing spatiotemporal variables measured for each individual $CD8^+$ T cell tracked over 12h. Each dot represents one cell. (**F**) Contact coefficient. (**G**) Mean speed of $CD8^+$ T cells measured in the absence of contact with fibrocytes ("Mean free speed"). (**H**) Mean speed of $CD8^+$ T cells measured in the presence of contact with fibrocytes ("Mean contact speed"). (**I, J, M, N**) Representative gating strategy for identification of $CD8^+$ T cells without (w/o) fibrocytes (**I, M**) or with (w) fibrocytes (**J, N**) in indirect (**I, J**) or direct (**M, N**) co-culture. Left panels: dot plots represent representative CD8-PerCP-Cy5-5 fluorescence (y-axis) versus side scatter (SSC, x-axis) of non-adherent cells removed from the culture. Right panels: histograms represent representative cell count (y-axis) versus Cell Trace-Pacific Blue fluorescence (x-axis). The distinct fluorescence peaks correspond to the different generations of $CD8^+$ T cells. The gate and the percentage indicate cells that have proliferated. (**K**, **O**) Comparison of manual count of non-adherent cells removed from co-culture without fibrocyte ("CD8") and with fibrocyte ("CD8+F"). L, (**P**) Comparison of quantifications of $CD8^+$ T cells that have proliferated, removed from co-culture without fibrocyte ("CD8") and with fibrocyte ("CD8+F"). (**B**, **D**, **F**, **G**, **H**, **K**, **L**, **O**, **P**) Medians are represented as horizontal lines. * $P < 0.05$, ** $P < 0.01$, *** $P < 0.001$. (**B**, **D**, **K**, **L**, **O**, **P**) Wilcoxon matched pairs test. (**F**, **G**, **H**) Mann Whitney tests.

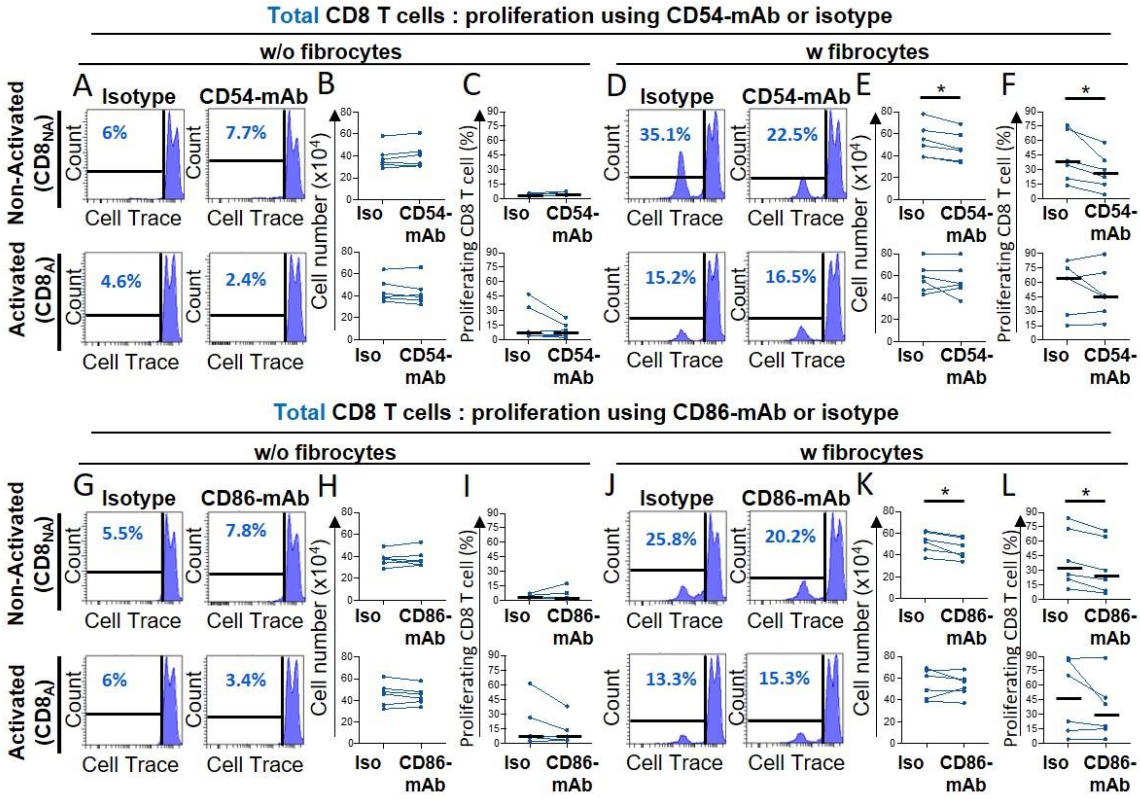

Fig. 4. Fibrocytes act as a major promoter on CD8$^+$ T cell proliferation in a CD54 and CD86-dependent manner. Prior to co-culture, CD8$^+$ T cells have been either non-activated ("$CD8_{NA}$") or activated ("$CD8_A$"). **(A**, **D**, **G**, **J)** Representative gating strategy for identification of proliferating CD8$^+$ T cells without (w/o) fibrocytes (**A**, **G**) or with (w) fibrocytes (**D**, **J**) using neutralizing CD54-mAb (**A**, **D**) or neutralizing CD86-mAb (**G**, **J**) and respective control isotype. Histograms represent representative cell count (y-axis) versus Cell Trace-Pacific Blue fluorescence (x-axis). The distinct fluorescence peaks correspond to the different generations of CD8$^+$ T cells. The gate and the percentage indicate cells that have proliferated. (**B**, **E**, **H**, **K**) Comparison of manual count of non-adherent cells removed from co-culture treated with neutralizing CD54-mAb or control isotype (Iso) (**B**, **E**) and neutralizing CD86-mAb or control isotype (Iso) (**H**, **K**). (**C**, **F**, **I**, **L**) Comparison of quantifications of CD8$^+$ T cells that have proliferated, removed from co-culture treated with neutralizing CD54-mAb (**C**, **F**) or neutralizing CD86-mAb (**I**, **L**) and respective control isotype. Medians are represented as horizontal lines. * $P < 0.05$, Wilcoxon matched pairs test.

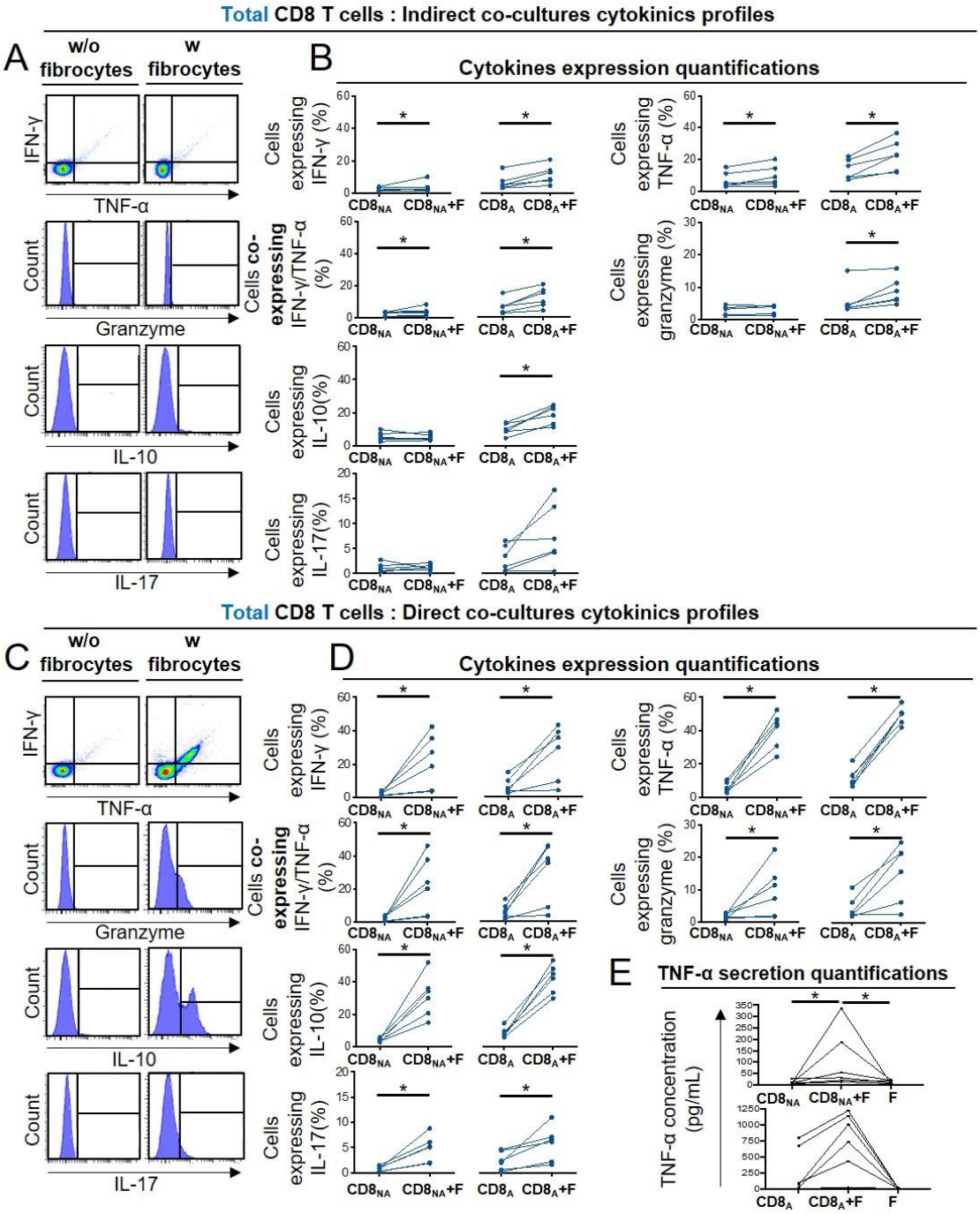

Fig. 5. Fibrocyte-CD8$^+$ T cell interactions alter cytokine production. Prior to co-culture, CD8$^+$ T cells have been either non-activated ("$CD8_{NA}$") or activated ("$CD8_A$"). (**A**, **C**) Representative gating strategy for identification of CD8$^+$ T cells expressing IFN- γ, TNF-α, granzyme, IL-10 and IL17 without (w/o) fibrocytes (left panel) or with (w) fibrocytes (right panel) in indirect (**A**) or direct (**C**) co-culture. (**B**, **D**) Quantifications of CD8$^+$ T cells expressing IFN-γ, TNF- α, both, granzyme and IL-10 after co-culture without fibrocytes ($CD8_{NA}$/$CD8_A$) or with fibrocytes ($CD8_{NA}$/$CD8_A$ +F) in indirect (**B**) or direct (**D**) co-culture. (**E**) TNF-α concentrations in supernatants from co-cultures without fibrocytes ($CD8_{NA}$/$CD8_A$), with fibrocyte ($CD8_{NA}$/$CD8_A$ +F), and only with fibrocytes (F) as control, for direct co-cultures. * $P < 0.05$, Wilcoxon matched pairs test, Friedman test.

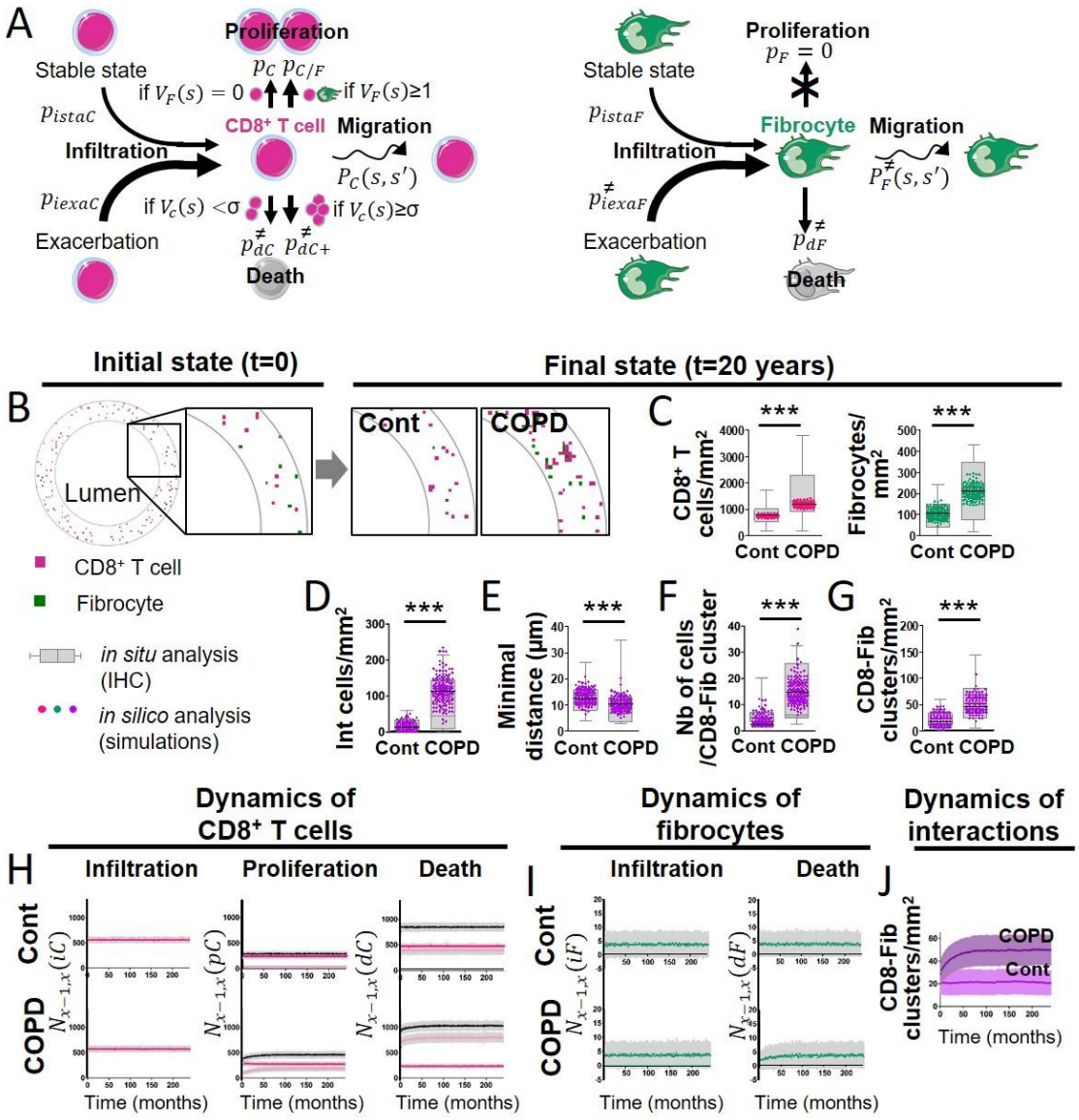

Fig. 6. A probabilistic cellular automata type model captures the features of the normal and pathological patterns of cell organisation observed in the tissues. (A) Schematic representation of the probabilities associated with CD8$^+$ T cells (left panel) and fibrocytes (right panel). For each CD8$^+$ T cell, we define a "basal" probability p_{dC} of dying, an increased probability p_{dC+} of dying when the CD8$^+$ T cell has many other CD8$^+$ T cells in its neighbourhood, a "basal" probability p_C of dividing, an increased probability $p_{C/F}$ of dividing when the CD8$^+$ T cell has fibrocytes in its neighbourhood, a probability $P_C\,(s,s')$ of moving from a site s to a neighboring site s', a probability p_{istaF} to be infiltrated at the stable state and a probability p_{iexaC} to be infiltrated during exacerbation. For each fibrocyte, we define a probability p_{dF} of dying, a probability p_F of dividing, a probability $P_F\,(s,s')$ of moving from a site s to a neighboring site s', a probability p_{istaF} to be infiltrated at the stable state and a probability p_{iexaF} to be infiltrated during exacerbation. The $\neq$ symbol indicates parameters whose numerical value differs from control to COPD situation. **(B)** Selected representative pictures for initial state and final states after 20 years of control and COPD dynamics. Images surrounded by black squares: higher magnifications of peribronchial area. CD8$^+$ T cells and fibrocytes are represented respectively by pink and green squares. **(C)** CD8$^+$ T cells (left) and fibrocyte (right) densities. **(D)** Interacting cells densities of interacting cells. **(E)** Mean minimal distances between fibrocyte and CD8$^+$ T

cells. (**F**) $CD8^+$ T cells-fibrocytes-containing clusters ("CD8-Fib clusters") densities. (**G**) mean number of cells by CD8-Fib clusters. (**C-G**), n=160 simulations for each situation. The medians are represented as horizontal lines. The equivalent measurements measured on patient's tissues are represented by gray boxes (25^{th} to the 75^{th} percentile) and whiskers (min to max). ***: P<0.001. unpaired t-tests or Mann-Whitney tests. (**H**, **I**) Mean kinetics of the populations of $CD8^+$ T cells and fibrocytes in control and COPD situation *in silico*. Standard deviations are indicated in gray, n=160 simulations. Left panels: $N_{x-1,x}(iC)$ and $N_{x-1,x}(iF)$ are the number of $CD8^+$ T cells (resp. fibrocytes) that have infiltrated the peribronchial area for the month x, relatively to the surface of interest. For fibrocytes, the infiltration at the stable state and during exacerbation are indicated respectively in green and light green. For control situation, there is no infiltration by exacerbation. Midde panels: $N_{x-1,x}(pC)$ is the number of $CD8^+$ T cells that have proliferated for the month x, relatively to the surface of interest. Basal duplication, fibrocyte-induced duplication and total duplication are indicated respectively in pink, light pink and black. Right panels: $N_{x-1,x}(dC)$ and $N_{x-1,x}(dF)$ are the number of $CD8^+$ T cells (resp. fibrocytes) that have died for the month x, relatively to the surface of interest. For $CD8^+$ T cells, basal death, T cell-induced death and total death are indicated respectively in pink, light pink and black. (**J**) Graphs showing the variations of the mean densities of CD8-Fib clusters over time in control (light purple) and COPD situation (dark purple).